

~~CONFIDENTIAL~~

RM A52L15a

NACA RM A52L15a

1049

0143525

TECH LIBRARY KAFB, NM



RESEARCH MEMORANDUM

EFFECT OF VERTICAL POSITION OF THE WING ON THE AERODYNAMIC
CHARACTERISTICS OF THREE WING-BODY COMBINATIONS

By John C. Heitmeyer

Ames Aeronautical Laboratory
Moffett Field, Calif.

Classification cancelled (or changed to) Unclassified

By Authority of: NASA Tech Rep Announcement #114
(OFFICER AUTHORIZED TO CHANGE)

By..... 22 Apr 57
NAME I.....

GRADE OF OFFICER MAKING CHANGE.....

3 Apr 61
DATE

**NATIONAL ADVISORY COMMITTEE
FOR AERONAUTICS**

WASHINGTON

February 18, 1953

**RECEIPT SIGNATURE
REQUIRED**

~~CONFIDENTIAL~~

1008/13



NATIONAL ADVISORY COMMITTEE FOR AERONAUTICS

RESEARCH MEMORANDUMEFFECT OF VERTICAL POSITION OF THE WING ON THE AERODYNAMIC
CHARACTERISTICS OF THREE WING-BODY COMBINATIONS

By John C. Heitmeyer

SUMMARY

Results are presented of an experimental investigation of three plane wings in combination with a body such that the models were representative of low- and high-wing arrangements. The three wings, having 3-percent-thick sections and of aspect ratio 3, had the following plan forms: a tapered unswept plan form, a tapered 45° swept-back plan form, and a triangular plan form. The lift, drag, and pitching-moment characteristics of each configuration were obtained for a range of Mach numbers from 0.61 to 0.91 and from 1.20 to 1.90. The results were obtained at constant Reynolds numbers per foot of 2.57 million and 4.00 million at all Mach numbers except 1.90. At this Mach number, data were obtained only at a Reynolds number per foot of 2.57 million. The results of this investigation at a Reynolds number per foot of 4.00 million are compared with results of tests of the same wings mounted in a midwing position on a body of revolution of the same axial distribution of cross-section area as the body employed in the present report. Results of the investigation show that only the drag characteristics were significantly affected by a change in the vertical location of the wing, the minimum drag coefficients of the midwing configurations being less than those of the respective high- and low-wing configurations. In general, the maximum lift-drag ratios of the low-wing configurations were less than either the midwing or high-wing configuration.

INTRODUCTION

The wealth of experimental data available concerned with the effect of the vertical position of the wing on the aerodynamic characteristics of wing-body combinations (hereinafter referred to as configurations) has been obtained, in general, at low subsonic Mach numbers with configurations employing relatively thick, high-aspect-ratio wings (e.g., ref. 1). To provide some experimental data of the effect of vertical position of the

wing on the aerodynamic characteristics of airplane-like wing-body configurations employing thin, low-aspect-ratio wings at high subsonic and supersonic speeds, an investigation of three plane wings in such combinations with a body as to represent low- and high-wing arrangements was undertaken. The wings were all 3 percent thick. The plan forms of the three wings included a tapered unswept plan form of aspect ratio 3.1, a tapered swept-back plan form of aspect ratio 3, and a triangular plan form of aspect ratio 3.

The results of tests of each wing in the midwing position have been published in references 2, 3, and 4. These results, together with the present experimental data, are compared to determine the effect of vertical displacement of the wing on the lift, drag, and pitching-moment characteristics of the combination.

NOTATION

b	wing span
\bar{c}	mean aerodynamic chord, $\frac{\int_0^{b/2} c^2 dy}{\int_0^{b/2} c dy}$
c	local wing chord
C_D	drag coefficient, drag/qS
C_L	lift coefficient, lift/qS
C_m	pitching-moment coefficient about a horizontal axis through the point on the body axis at the body station corresponding to the quarter point of the mean aerodynamic chord, pitching moment/qS \bar{c} (See fig. 1.)
L/D	lift-drag ratio
$(L/D)_{\max}$	maximum lift-drag ratio
M	Mach number
q	free-stream dynamic pressure
R	Reynolds number based on mean aerodynamic chord
S	total wing area including area formed by extending the leading edge and trailing edge to the plane of symmetry

y distance perpendicular to plane of symmetry
 $dC_L/d\alpha$ slope of the lift curve measured at zero lift, per deg
 dC_m/dC_L slope of the pitching-moment curve measured at zero lift
 α angle of attack of the body axis, deg

APPARATUS

Wind Tunnel and Balance

The data of the present report were obtained in the Ames 6- by 6-foot supersonic wind tunnel. In this wind tunnel, the Mach number can be varied continuously and the stagnation pressure regulated to maintain a given test Reynolds number. The quantity of water vapor present in the tunnel air was small enough to prevent formation of condensation shocks at all supersonic Mach numbers. Further information about this wind tunnel is presented in reference 5.

The models were sting-mounted in the wind tunnel, the diameter of the straight sting being about 93 percent of the diameter of the body base. The model support permitted tests through an angle-of-attack range from -17° to 17° in a horizontal plane. The 4-inch-diameter, four-component, strain-gage balance described in reference 6 was enclosed within the body of each model and was used to measure the aerodynamic forces and moments.

Model

Plan views of each model, a typical front view, and certain model dimensions are given in figure 1. A photograph of the swept-back-wing model is shown in figure 2. This swept-back wing and the unswept and triangular wings of the present investigation are the same wings that were used in the tests reported in references 2, 3, and 4. A summary of the important geometric characteristics of each model is presented in table I.

To facilitate the mounting of the wings in the off-center-line position, it was necessary to modify the circular cross section of the body of revolution used in references 2, 3, and 4. The cross sections of the body of the present report (fig. 3) were derived in a manner so as to obtain a related shape having the same cross-sectional area as the sections of the body of revolution. The noncircular cross sections of

the modified body were made up of four parabolic arcs. Figure 3 shows a typical section and indicates the control points and tangents to the sections which are necessary for the construction of the arcs. Included in figure 3 is a table which lists the location of the control points and the angle of the tangents to the section for the different cross sections at the various body stations.

A fillet which consisted of concentric radii was used to fair the upper surface of the wing to the modified body. The type of fillet can be seen from figure 4 which presents three cross sections of the triangular-wing model. It should be mentioned here that the models of references 2, 3, and 4 (the midwing configurations) employed no fillets at the wing-body juncture.

The wings of each model were solid steel. The body, with the exception of an aluminum nose section, was also solid steel. A tin-bismuth alloy was used to form the required fillets between the wing and body. All exposed model surfaces were polished smooth.

TESTS AND PROCEDURE

Range of Test Variables

The lift, drag, and pitching moment of each model were investigated for a range of Mach numbers from 0.61 to 0.91 and from 1.20 to 1.90. The data of each model were obtained at constant Reynolds numbers per foot of 2.57 million and 4.00 million for all Mach numbers except 1.90. At this Mach number, wind-tunnel power limited the test Reynolds number per foot to 2.57 million.

The model support permitted tests to a maximum angle of 17° in the horizontal plane. By testing through the angle range from -17° to 17° , the aerodynamic characteristics of a given configuration could be studied as both a low- and high-wing arrangement.

Reduction of Data

The test data have been reduced to standard NACA coefficient form. Factors which could affect the accuracy of these results, together with the corrections applied, are discussed in the following paragraphs.

Tunnel-wall interference.- Corrections to the subsonic results for the induced effects of the tunnel walls were made according to the methods

of reference 7. The numerical values of these corrections (which were added to the uncorrected data) for each model were obtained from:

<u>Unswept-wing model</u>	<u>Swept-back-wing model</u>	<u>Triangular-wing model</u>
$\Delta\alpha = 0.57 C_L$	$\Delta\alpha = 0.55 C_L$	$\Delta\alpha = 0.55 C_L$
$\Delta C_D = .0100 C_L^2$	$\Delta C_D = .0097 C_L^2$	$\Delta C_D = .0097 C_L^2$

No corrections were made to the pitching-moment data for this effect.

The effects of constriction of the flow at subsonic speeds by the tunnel walls were taken into account by the method of reference 8. This correction was calculated for conditions at zero angle of attack and was applied throughout the angle-of-attack range. This correction was the same for each model and, at a Mach number of 0.91, amounted to about a 2-percent increase in the Mach number and in the dynamic pressure over that determined from a calibration of the wind tunnel without a model in place.

During the tests at supersonic speeds, the Mach wave originating at the nose of the model did not reflect from the tunnel walls back across the model. No corrections were required, therefore, for tunnel-wall effects.

Support interference.- At subsonic speeds, the effects of support interference on the aerodynamic characteristics of the present models are not known. For these tailless models, it is believed that such effects consisted primarily of a change in the pressure at the base of each model. In an effort to correct at least partially for this support interference, the base pressure was measured and the drag data adjusted to correspond to a base pressure equal to the static pressure of the free stream.

At supersonic speeds, the effects of support interference on a body-sting configuration similar to that of the present model are shown by reference 9 to be confined to a change in base pressure. The previously mentioned adjustment of the drag for base pressure was applied, therefore, at supersonic speeds. It should be noted that the drag coefficients as presented in the present report are, in essence, foredrag coefficients since the base drag is not included.

Effect of Stream Characteristics

Subsonic Mach number calibration.- The recent and thorough calibration of the 6- by 6-foot supersonic wind tunnel at subsonic speeds indicated a small change from the previous subsonic Mach number calibration.

Both the data of references 2, 3, and 4 presented in this report and the data obtained during the present investigation have been based upon this latest calibration. The magnitude of the change in Mach number and the ratio of the dynamic pressures are as follows:

M_{old}	M_{new}	q_{old}/q_{new}
0.60	0.61	0.974
.70	.71	.980
.80	.81	.982
.90	.91	.987

Axial static-pressure gradient.— The recent survey of the air stream in the 6- by 6-foot supersonic wind tunnel at subsonic speeds also indicates that the static-pressure gradient present in the test section is of sufficient magnitude to affect the drag results. A similar effect at supersonic speeds has been indicated by the results of the survey of reference 5. Therefore, a correction, C_{Dg} , was added to the measured drag coefficients at all test Mach numbers to account for the longitudinal buoyancy caused by the axial static-pressure variation. This correction will be the same for each model of the present report since only the effect of the static-pressure variation on the body was considered. The correction for the models of the present report at the various test Mach numbers is as follows:

M	C_{Dg}	M	C_{Dg}
0.61	0.0002	1.20	0
.71	.0002	1.40	-.0003
.81	.0003	1.50	.0003
.91	.0005	1.70	.0010
----	-----	1.90	.0006

Only the supersonic drag data presented in references 2, 3, and 4 have had the correction applied to them to account for the effect of the longitudinal buoyancy. The subsonic drag coefficients of these investigations have been corrected in the present report to account for this effect. The magnitude of the correction, C_{Dg} , at the various test Mach numbers for the models of references 2, 3, and 4 is as follows:

M	C_{Dg}	M	C_{Dg}
0.61	0.0001	1.20	0.0002
.71	.0002	1.40	0
.81	.0002	1.50	.0003
.91	.0007	1.70	.0006
----	-----	1.90	.0006

The fact that the models of references 2, 3, and 4 were located 1 inch farther upstream in the test section than the models of the present report accounts for the different values of C_{Dg} at a given Mach number.

Stream inclination and stream curvature.- Results of tests of the swept-back-midwing configuration (ref. 3) and of the triangular-midwing configuration (ref. 4) in both the upright and inverted test positions have indicated that a stream inclination of -0.05° and a stream curvature capable of producing a pitching-moment coefficient of -0.004 at zero lift exists in the tunnel air stream at subsonic speeds. Results of like tests of the present model employing the swept-back wing mounted in an off-center-line wing position indicate a stream inclination of -0.07° and a stream curvature capable of producing a pitching-moment coefficient of -0.002 at zero lift. No tests were made with the models employing the unswept wing or triangular wing mounted in an off-center-line wing position for the purposes of determining the magnitude of the stream irregularities. As noted above, and as noted in references 2 and 10, the magnitude of these stream irregularities are different for different model configurations. Since no data indicating the magnitude of the irregularities are available for the models with the unswept wing and triangular wing mounted in an off-center-line wing position and since no method for correcting the drag data for the effects of the indicated stream curvature is known, no attempt was made to change the data presented in this report for the effects of stream inclination and stream curvature.

RESULTS

The basic data of the present investigation for the unswept-wing model, the swept-back-wing model, and the triangular-wing model are presented in figures 5, 6, and 7, respectively. In these figures, the variation of lift coefficient with angle of attack, and the variation of drag coefficient, pitching-moment coefficient, and lift-drag ratio with lift coefficient for the various test Mach numbers and Reynolds numbers are presented for each model. A comparison of the aerodynamic characteristics of each wing in combination with the body in a low-, mid-, and high-wing position is presented in figures 8, 9, and 10. The results presented in these figures have been summarized in figures 11, 12, and 13, respectively, to show some important parameters as functions of Mach number. The data of the high-wing configurations were obtained from the negative angle-of-attack data of the low-wing configurations.

The data presented in figures 5 through 10 have been tabulated and are presented in tables II and III.

Effect of Reynolds Number

The basic data of figures 5, 6, and 7 indicate that only the drag and pitching-moment characteristics of the unswept-wing configurations and the lift and pitching-moment characteristics of the swept-back-wing configurations were affected by the change in the test Reynolds number. An increase in the minimum drag coefficient of the unswept-low-wing configurations occurred at all test Mach numbers as the Reynolds number increased from 2.4 million to 3.8 million. This effect of a change in Reynolds number on the minimum drag can also be noted in the data of reference 2 for the unswept-midwing configuration and is probably due to the transition point of the boundary layer moving forward on the wing with increasing Reynolds number.

The effect of the change in Reynolds number on the pitching-moment characteristics of the unswept- and the swept-back-wing model was limited to results obtained at subsonic speeds and in particular to results obtained near zero lift. The variation of the pitching-moment coefficient with lift coefficient for each model was nonlinear near zero lift (C_L of -0.1 to $+0.1$) at a Reynolds number per foot of 2.57 million, the data indicating a forward shift in the position of the center of pressure. This nonlinear variation was not present, however, in the data obtained for each model at a Reynolds number per foot of 4.00 million. Similar effects of Reynolds number upon the variation of pitching moment with lift can readily be seen from the data of references 2 and 3, and are attributed to a combination of boundary-layer and terminal-shock effects upon the chordwise pressure distribution of the biconvex airfoil section. A discussion of this flow phenomenon may be found in reference 11.

The data obtained for the swept-back-low-wing model at Mach numbers of 1.20 and 1.70 indicate a decrease in the value of the lift-curve slope with an increase in Reynolds number from 2.5 million to 3.8 million. The data of the swept-back-midwing model (ref. 3) at a Mach number of 1.70 show the same variation in the value of lift-curve slope with Reynolds number. Although the effect of aeroelastic bending, associated with the larger values of dynamic pressure at the higher Reynolds number, would tend to decrease the lift-curve slope, it is believed that the elastic deformation of the wing is not the principal cause of the variation of lift-curve slope with Reynolds number; therefore, at present the full reason for the decrease in the value of the lift-curve slope is not known.

Effect of Vertical Position of Wing

Unswept-wing configurations.— Examination of the data of figures 8 and 11 indicate that of the characteristics presented, lift, drag, and pitching moment, only the drag was significantly affected by a change in

~~CONFIDENTIAL~~

the vertical position of the wing. The effect upon the lift and pitching moment was, in general, small and of secondary importance.

The displacement of the unswept wing from the midwing position to either the low- or high-wing position resulted in an increase in the minimum drag coefficient, particularly at supersonic speeds where a difference of 0.0020 is indicated (fig. 11(d)). It is interesting to note that despite the larger value of minimum drag, the unswept-high-wing configuration had a larger maximum lift-drag ratio than the unswept-midwing configuration at all test Mach numbers except 1.50 and 1.90. The results indicate the existence of a favorable wing-body interference effect at angle of attack for the high-wing configuration (figs. 11(c) and 11(d)).

The effect of vertical position of the wing on the lift and pitching-moment characteristics of the unswept-wing configurations was, as mentioned previously, small. The variations of lift coefficient with angle of attack and of pitching-moment coefficient with lift coefficient for both the high- and low-wing configurations at subsonic speeds were more linear near zero lift than those of the midwing configurations. At all speeds, the midwing configurations had a somewhat smaller value of lift-curve slope at zero lift than either the high- or low-wing configurations.

Swept-back-wing configuration.- The data for the swept-back-wing configuration presented in figures 9 and 12 indicate that the drag characteristics were most affected by a change in the vertical position of the wing relative to the body center line. The lift and pitching-moment characteristics were not appreciably affected.

Throughout the range of test Mach numbers, the midwing configuration had a smaller value of minimum drag than either the high- or low-wing configuration. As was the case for the unswept-wing configuration, the differences in minimum drag were more pronounced at the supersonic Mach numbers. The data of figure 9(d) show that the midwing configuration had the larger value of maximum lift-drag ratio throughout the range of test Mach numbers. Calculations indicate that the differences in the maximum lift-drag ratios cannot be attributed entirely to the larger values of minimum drag of the high- and low-wing configurations, thereby indicating that the midwing configurations had a favorable wing-body interference effect at angles of attack.

The variation of lift coefficient with angle of attack and the variation of pitching-moment coefficient with lift coefficient for the swept-back-wing configuration, as shown in figures 9(a) and 9(b), were practically the same for each vertical position of the wing.

Triangular-wing configuration.- As shown in figures 10 and 13, the lift and pitching-moment characteristics of the triangular-wing

configuration were not appreciably affected by a change in the vertical position of the wing. The results indicate, however, that the minimum drag coefficients of the midwing configuration were slightly smaller, and that the maximum lift-drag ratios of the midwing configuration were larger than those of the high- and low-wing configurations.


The data presented in figures 8(c), 9(c), and 10(c) show that the minimum drag coefficient of the triangular-wing models was the least affected by a change in the vertical position of the wing. The smaller change indicated for the triangular-wing models is believed to be related to the fact that the wing-body juncture was aerodynamically more efficient, due to the longer root chord, than those of the unswept- and swept-back-wing models.

CONCLUSIONS

The results of a wind-tunnel investigation between the Mach numbers of 0.61 and 0.91, 1.20 and 1.90 of three aspect ratio 3 wings, each mounted in a midwing position on a body of revolution and in a high- and a low-wing position on a modified body of the same axial distribution of cross-sectional area as the body of revolution indicate that:

1. The variations of lift coefficient with angle of attack and of pitching moment with lift coefficient for each model of a given plan form were not greatly affected by a change in the vertical location of the wing. The displacement of the unswept wing to a high- or a low-wing position eliminated the slight nonlinearity near zero lift present in the lift and pitching-moment data of the midwing models.
2. The minimum drag coefficient of the midwing configurations were less than those of the respective high- and low-wing configurations. The minimum drag of the triangular-wing models showed the least change with the different vertical wing positions.
3. In general, the maximum lift-drag ratios of the low-wing configurations were somewhat less than those of the midwing or high-wing configurations.

Ames Aeronautical Laboratory
National Advisory Committee for Aeronautics
Moffett Field, Calif.



REFERENCES

1. Jacobs, Eastman N., and Ward, Kenneth E.: Interference of Wing and Fuselage from Tests of 209 Combinations in the NACA Variable-Density Tunnel. NACA Rep. 540, 1935.
2. Reese, David E., and Phelps, E. Ray: Lift, Drag, and Pitching Moment of Low-Aspect-Ratio Wings at Subsonic and Supersonic Speeds - Plane Tapered Wing of Aspect Ratio 3.1 with 3-Percent-Thick, Biconvex Section. NACA RM A50K28, 1951.
3. Heitmeyer, John C.: Lift, Drag, and Pitching Moment of Low-Aspect-Ratio Wings at Subsonic and Supersonic Speeds - Plane 45° Swept-Back Wing of Aspect Ratio 3, Taper Ratio 0.4 with 3-Percent-Thick, Biconvex Section. NACA RM A51H10, 1951.
4. Heitmeyer, John C.: Lift, Drag, and Pitching Moment of Low-Aspect-Ratio Wings at Subsonic and Supersonic Speeds - Plane Triangular Wing of Aspect Ratio 3 with NACA 0003-63 Section. NACA RM A51H02, 1951.
5. Frick, Charles W., and Olson, Robert N.: Flow Studies in the Asymmetric Adjustable Nozzle of the Ames 6- by 6-Foot Supersonic Wind Tunnel. NACA RM A9E24, 1949.
6. Olson, Robert N., and Mead, Merrill H.: Aerodynamic Study of a Wing-Fuselage Combination Employing a Wing Swept Back 63° . Effectiveness of an Elevon as a Longitudinal Control and the Effects of Camber and Twist on the Maximum Lift-Drag Ratio at Supersonic Speeds. NACA RM A50A31a, 1950.
7. Silverstein, Abe and White, James A.: Wind-Tunnel Interference with Particular Reference to Off-Center Positions of the Wing and to the Downwash at the Tail. NACA Rep. 547, 1935.
8. Herriot, John G.: Blockage Corrections for Three-Dimensional-Flow Closed-Throat Wind Tunnels, with Consideration of the Effect of Compressibility. NACA Rep. 995, 1950. (Supersedes NACA RM A7B28)
9. Perkins, Edward W.: Experimental Investigation of the Effects of Support Interference on the Drag of Bodies of Revolution at a Mach Number of 1.5. NACA TN 2292, 1951.
10. Hall, Charles F., and Heitmeyer, John C.: Lift, Drag, and Pitching Moment of Low-Aspect-Ratio Wings at Subsonic and Supersonic Speeds - Twisted and Cambered Triangular Wing of Aspect Ratio 2 with NACA 0003-63 Thickness Distribution. NACA RM A51E01, 1951.

11. Dugan, Duane W.: Effects of Three Types of Blunt Trailing Edges on the Aerodynamic Characteristics of a Plane Tapered Wing of Aspect Ratio 3.1, With a 3-Percent-Thick Biconvex Section. NACA RM A52E01, 1952.

TABLE I.- GEOMETRIC CHARACTERISTICS OF THE MODELS

Characteristic	Unswept-wing model	Swept-back wing model	Triangular wing model
Aspect Ratio	3.1	3.0	3.0
Taper Ratio	0.39	0.4	0
Airfoil Section (streamwise)	3% thick, biconvex	3% thick, biconvex	NACA 0003-63
Dihedral, degrees	0	0	0
Incidence, degrees	0	0	0
Total wing area, S, square feet	2.425	2.425	2.425
Mean aerodynamic chord, \bar{c} , feet	0.944	0.956	1.199
Distance wing chord plane to body axis, \bar{x} /mean aerodynamic chord	17.5	17.3	13.8

TABLE II.- AERODYNAMIC CHARACTERISTICS OF THE MIDWING-BODY COMBINATIONS¹
[Reynolds number per foot, 4.00 million]

Unswept-wing model																			
M	α	C_L	C_D	C_m	M	α	C_L	C_D	C_m	M	α	C_L	C_D	C_m	M	α	C_L	C_D	C_m
0.61	-0.31	-0.021	0.0078	-0.003	0.71	-4.82	-0.337	0.0914	-0.022	0.81	0.63	0.031	0.0090	0.003	1.20	-4.78	-0.381	0.0470	0.048
	-0.68	-0.037	0.0077	-0.005		-5.96	-0.423	0.0478	-0.016		1.28	-0.068	0.0093	0.007		-5.93	-0.477	0.0521	0.053
	-1.27	-0.083	0.0083	-0.007		-7.13	-0.529	0.0714	-0.016		2.21	0.156	0.0156	0.013		-4.40	-0.099	0.0150	0.005
	-2.43	-0.157	0.0120	-0.011		-9.37	-0.682	0.1237	-0.078		9.71	0.293	0.0215	0.023		32	0.018	0.0163	0.008
	-3.99	-0.258	0.0182	-0.015		-11.42	-0.714	0.1558	-0.102		4.89	0.368	0.0329	0.027		68	0.043	0.0167	-0.005
	-4.73	-0.314	0.0279	-0.018		-9.39	-0.698	0.1280	-0.085		6.09	0.450	0.0492	0.034		1.29	0.089	0.0175	-0.010
	-5.84	-0.381	0.0386	-0.024		1.29	0.009	0.0069	0.001		2.88	0.189	0.0236	0.023		2.88	0.189	0.0236	-0.023
	-6.96	-0.468	0.0508	-0.031		1.23	0.064	0.0092	0.006		3.64	0.276	0.0394	0.034		3.64	0.276	0.0394	-0.034
	-8.20	-0.621	0.0707	-0.041		2.46	0.148	0.0132	0.010		4.77	0.362	0.0564	0.045		4.77	0.362	0.0564	-0.045
	-11.31	-0.690	0.1469	-0.073		3.63	0.238	0.0202	0.015		5.90	0.454	0.0738	0.059		5.90	0.454	0.0738	-0.059
	2.29	0.009	0.0082	0		4.79	0.318	0.0303	0.020		6.09	0.450	0.0492	0.034		7.04	0.545	0.0842	-0.071
	1.60	0.066	0.0089	0.002		5.93	0.400	0.0440	0.021		-3.88	-0.324	0.0293	-0.024		-3.88	-0.324	0.0293	-0.024
	1.21	0.084	0.0086	0.002		7.07	0.479	0.0615	0.016		-5.15	-0.407	0.0333	-0.027		-5.15	-0.407	0.0333	-0.027
	2.40	0.138	0.0121	0.004		9.33	0.686	0.1063	-0.066		6.43	0.642	0.0310	-0.021		6.43	0.642	0.0310	-0.021
	3.56	0.218	0.0185	0.012		11.40	0.777	0.1458	-0.046		-8.65	-0.204	0.0325	-0.023		-8.65	-0.204	0.0325	-0.023
	4.70	0.297	0.0278	0.015		13.48	0.706	0.1818	-0.069		1.31	0.012	0.0021	0.002		1.31	0.012	0.0021	0.002
	5.83	0.371	0.0398	0.019		14.45	0.712	0.2013	-0.078		6.66	0.037	0.0094	0.005		6.66	0.037	0.0094	0.005
	6.95	0.446	0.0536	0.018		17.50	0.740	0.2532	-0.088		1.33	0.053	0.0107	0.009		1.33	0.053	0.0107	0.009
9.19	0.597	0.0808	0.028	0.81	-3.5	-0.029	0.0081	-0.004	1.20	3.88	0.200	0.0197	0.019	1.50	-3.33	-0.028	0.0187	0.003	
11.31	0.777	0.1422	0.041		-1.33	-0.059	0.0087	-0.009		5.15	0.407	0.0333	0.027		-4.67	-0.029	0.0130	0.006	
13.33	0.700	0.1773	0.059		-2.54	-0.178	0.0135	-0.016		6.33	0.570	0.0584	0.052		-1.26	-0.070	0.0145	0.012	
15.35	0.713	0.2110	0.081		-3.75	-0.277	0.0220	-0.022		7.31	0.670	0.0997	0.039		-2.40	-0.141	0.0192	0.008	
17.38	0.731	0.2469	0.086		-4.94	-0.374	0.0398	-0.021		8.65	0.700	0.0217	0.024		-3.53	-0.210	0.0265	0.025	
-0.34	-0.023	0.0082	-0.003		6.18	0.519	0.0626	0.022		1.33	0.053	0.0107	0.009		4.64	-0.273	0.0328	0.045	
-0.66	-0.042	0.0082	-0.004		6.16	0.510	0.0613	0.018		1.36	0.059	0.0157	0.017		5.78	-0.340	0.0461	0.055	
-1.31	-0.084	0.0089	-0.006		-2.34	-0.022	0.0080	-0.004		5.08	0.434	0.0420	0.029		9.07	-0.538	0.1003	0.100	
-2.50	-0.167	0.0130	-0.012		-3.5	-0.029	0.0081	-0.004		5.08	0.434	0.0420	0.029		9.07	-0.538	0.1003	0.100	
-3.68	-0.256	0.0208	-0.017		-4.67	-0.307	0.0314	-0.038		6.33	0.570	0.0584	0.052		5.78	-0.340	0.0461	0.055	
					-5.84	-0.381	0.0386	-0.024		7.31	0.670	0.0997	0.039		-3.53	-0.028	0.0187	0.003	
					-6.96	-0.468	0.0508	-0.031		8.65	0.700	0.0217	0.024		3.33	-0.011	0.0187	0.001	
					-8.20	-0.621	0.0707	-0.041		9.71	0.293	0.0215	0.023		4.67	-0.029	0.0130	0.006	
					-11.31	-0.690	0.1469	-0.073		1.26	0.018	0.0163	0.008		1.26	0.018	0.0163	0.008	
										2.39	0.133	0.0192	0.012		2.39	0.133	0.0192	0.012	
										3.52	0.201	0.0261	0.023		3.52	0.201	0.0261	0.023	
										4.63	0.266	0.0354	0.033		4.63	0.266	0.0354	0.033	
Swept-back-wing model																			
M	α	C_L	C_D	C_m	M	α	C_L	C_D	C_m	M	α	C_L	C_D	C_m	M	α	C_L	C_D	C_m
0.61	-0.60	-0.058	0.0067	-0.001	0.81	-1.80	-0.095	0.0098	0.008	0.91	-4.78	-0.399	0.0366	0.038	1.20	2.18	0.142	0.0175	-0.026
	-1.27	-0.083	0.0077	0		-2.33	-0.173	0.0137	0.005		-5.68	-0.503	0.0561	0.062		3.88	0.221	0.0233	-0.040
	-2.43	-0.157	0.0121	0.001		-3.48	-0.260	0.0206	0.010		5.68	0.503	0.0561	0.062		4.36	0.298	0.0316	-0.050
	-3.98	-0.258	0.0181	0.004		-4.63	-0.348	0.0317	0.018		1.17	0.072	0.0089	0.004		5.47	0.377	0.0427	-0.072
	-4.90	-0.312	0.0263	0.004		-5.71	-0.431	0.0460	0.024		2.33	0.169	0.0127	0.012		6.57	0.458	0.0572	-0.098
	-5.61	-0.391	0.0411	0.014		6.4	0.022	0	3.50		0.260	0.0202	0.022	-5.6		-0.045	0.0149	0.008	
	-6.95	-0.518	0.0685	0		1.14	0.062	0.0085	-0.002		4.67	0.367	0.0314	0.038		-1.10	-0.076	0.0158	0.011
	1.08	0.056	0.0087	-0.001		2.86	0.142	0.0120	0.006		5.83	0.471	0.0468	0.059		2.19	0.141	0.0190	0.006
	2.22	0.127	0.0117	-0.004		3.38	0.225	0.0176	0.010		6.96	0.544	0.0667	0.065		-2.19	-0.141	0.0190	0.006
	3.33	0.200	0.0164	0.005		4.77	0.316	0.0270	0.018		-2.27	-0.207	0.0246	0.024		3.27	0.207	0.0246	0.024
	4.45	0.281	0.0241	0.010		5.71	0.402	0.0403	0.029		4.35	0.270	0.0328	0.035		4.35	0.270	0.0328	0.035
	5.59	0.377	0.0333	0.015		6.83	0.474	0.0563	0.042		-2.12	-0.092	0.0126	0.016		-3.44	-0.334	0.0431	0.059
	6.67	0.433	0.0501	0.019		9.04	0.592	0.0933	0.088		2.22	0.169	0.0127	0.012		5.4	0.086	0.0150	-0.002
	8.87	0.561	0.0863	0.026		-1.66	-0.064	0.0089	0.001		-3.31	-0.248	0.0260	0.044		1.08	0.059	0.0153	-0.012
	11.03	0.668	0.1282	0.032		-2.43	-0.105	0.0104	0.005		-4.41	-0.344	0.0393	0.060		2.16	0.124	0.0178	-0.004
	13.16	0.758	0.1762	0.039		-3.48	-0.196	0.0190	0.011		-5.51	-0.402	0.0478	0.079		3.25	0.189	0.0228	-0.038
	-0.66	-0.058	0.0089	0		-4.63	-0.260	0.0206	0.010		1.08	0.059	0.0153	0.012		4.33	0.294	0.0300	-0.052
						-5.71	-0.348	0.0317	0.018		2.33	0.169	0.0127	0.012		5.42	0.317	0.0394	-0.067
0.81	-0.60	-0.058	0.0067	-0.001	0.91	-1.80	-0.095	0.0098	0.008	1.20	-4.78	-0.399	0.0366	0.038	1.50	-0.54	-0.040	0.0164	0.010
	-1.27	-0.083	0.0077	0		-2.33	-0.173	0.0137	0.005		-5.68	-0.503	0.0561	0.062		-1.07	-0.059	0.0136	0.017
	-2.43	-0.157	0.0121	0.001		-3.48	-0.260	0.0206	0.010		1.17	0.072	0.0089	0.004		-2.14	-0.189	0.0173	0.038
	-3.98	-0.258	0.0181	0.004		-4.63	-0.348	0.0317	0.018		2.33	0.169	0.0127	0.012		3.21	-0.186	0.0225	0.046
	-4.90	-0.312	0.0263	0.004		-5.71	-0.431	0.0460	0.024		3.50	0.260	0.0202	0.022		4.28	-0.246	0.0296	0.061
	-5.61	-0.391	0.0411	0.014		6.4	0.022	0											

Triangular-wing model																			
M	α	C_L	C_D	C_m	M	α	C_L	C_D	C_m	M	α	C_L	C_D	C_m	M	α	C_L	C_D	C_m
0.61	-0.57	-0.048	0.0083	0.004	0.91	-0.62	-0.058	0.0080	0.009	1.20	-0.55	-0.048	0.0122	0.012	1.50	-0.54	-0.040	0.0164	0.010
	-1.10	-0.074	0.0090	0.007		-1.15	-0.094	0.0089	0.012		-1.05	-0.061	0.0134	0.013		-1.07	-0.059	0.0136	0.017
	-2.19	-0.136	0.0141	0.014		-2.17	-0.171	0.0127	0.006		-2.17	-0.171	0.0127	0.006		-2.14	-0.189	0.0173	0.038
	-3.99	-0.258	0.0181	0.009		-3.40	-0.262	0.0208	0.018		-3.44	-0.221	0.0229	0.020		-3.81	-0.186	0.0225	0.046
	-4.87	-0.260	0.0230	0.016		-4.51	-0.286	0.0297	0.049		-4.38	-0.290	0.0313	0.078		-4.28	-0.246	0.0296	0.061
	-5.44	-0.321	0.0340	0.031		-5.65	-0.309	0.0461	0.065		-5.39	-0.339	0.0481	0.089		-5.34	-0.303	0.0470	0.098
	3.33	0.022	0.0079	-0.004		5.55	0.028	0.0070	-0.004		5.23	0.022	0.0118	-0.005		5.2	0.023	0.0121	-0.006
	1.07	0.093	0.0083	-0.008		1.10	0.067	0.0080	-0.012		1.07	0.099	0.0126	-0.013		1.06	0.093	0.0126	-0.013
	2.22	0.133	0.0126	-0.019		2.13	0.145	0.014	-0.028		2.14	0.137	0.0137	-0.030		2.18	0.133	0.0163	-0.028
	3.34	0.173	0.0184	-0.021		3.35	0.223	0.0173	-0.037		3.22	0.198	0.0209	-0.043		3.20	0.173	0.0218	-0.043
	4.32	0.235	0.0240	-0.027		4.48	0.307	0.0269	-0.054		4.29	0.267	0.0284	-0.066		4.27	0.231	0.0278	-0.057
	5.41	0.300	0.0355	-0.033		5.63	0.393	0.0397	-0.062		5.37	0.338	0.0386	-0.083		5.32	0.286	0.0363	-0.070
	6.57	0.365	0.0455	-0.038		6.73	0.460	0.0517	-0.076		6.41	0.406	0.0512	-0.100		6.39	0.339	0.0475	-0.085
	8.87	0.472	0.0713	-0.040		8.18	0.598	0.0709	-0.092		7.45	0.607	0.0690	-					

TABLE III.- AERODYNAMIC CHARACTERISTICS OF THE LOW-WING-BODY COMBINATIONS
(a) Reynolds number per foot, 2.57 million

NACA

TABLE III.- AERODYNAMIC CHARACTERISTICS OF THE LOW-WING-BODY
COMBINATIONS - Concluded
(b) Reynolds numbers per foot, 4.00 million

Unswpt-wing model																			
M	α	C_L	C_D	C_M	M	α	C_L	C_D	C_M	M	α	C_L	C_D	C_M	M	α	C_L	C_D	C_M
0.61	-0.30	-0.022	0.0086	-0.007	0.71	-0.61	-0.044	0.0086	-0.009	0.81	-1.24	-0.093	0.0098	-0.016	0.91	-1.78	-0.346	0.0270	-0.043
	-0.59	-0.041	0.0086	-0.008		-0.91	-0.064	0.0086	-0.011		-1.51	-0.139	0.0111	-0.019		-2.04	-0.486	0.0484	-0.039
	-0.88	-0.059	0.0086	-0.010		-1.21	-0.083	0.0093	-0.014		-1.80	-0.179	0.0137	-0.022		-2.30	-0.624	0.0698	-0.045
	-1.15	-0.075	0.0093	-0.011		-1.47	-0.121	0.0106	-0.015		-2.00	-0.222	0.0173	-0.026		-2.61	-0.861	0.0927	-0.051
	-1.44	-0.114	0.0105	-0.015		-1.75	-0.161	0.0130	-0.016		-2.29	-0.268	0.0215	-0.029		-2.90	-1.093	0.1161	-0.058
	-1.74	-0.152	0.0127	-0.017		-2.03	-0.203	0.0160	-0.022		-2.50	-0.317	0.0244	-0.035		-3.19	-1.324	0.1400	-0.065
	-2.03	-0.190	0.0154	-0.020		-2.30	-0.243	0.0196	-0.025		-2.80	-0.367	0.0273	-0.038		-3.49	-1.556	0.1639	-0.072
	-2.31	-0.229	0.0181	-0.023		-2.58	-0.283	0.0230	-0.028		-3.09	-0.416	0.0302	-0.041		-3.78	-1.788	0.1878	-0.079
	-2.60	-0.267	0.0208	-0.026		-2.86	-0.323	0.0260	-0.031		-3.38	-0.465	0.0331	-0.044		-4.07	-2.020	0.2117	-0.086
	-2.89	-0.305	0.0235	-0.029		-3.15	-0.363	0.0290	-0.034		-3.67	-0.514	0.0360	-0.047		-4.36	-2.252	0.2356	-0.093
	-3.18	-0.343	0.0262	-0.032		-3.44	-0.403	0.0320	-0.037		-3.96	-0.563	0.0389	-0.050		-4.65	-2.484	0.2595	-0.100
	-3.47	-0.381	0.0289	-0.035		-3.73	-0.443	0.0350	-0.040		-4.25	-0.612	0.0418	-0.053		-4.94	-2.716	0.2834	-0.107
	-3.76	-0.419	0.0316	-0.038		-4.02	-0.483	0.0380	-0.043		-4.54	-0.661	0.0447	-0.056		-5.23	-2.948	0.3073	-0.114
	-4.05	-0.457	0.0343	-0.041		-4.31	-0.523	0.0410	-0.046		-4.83	-0.710	0.0476	-0.059		-5.52	-3.180	0.3312	-0.121
	-4.34	-0.495	0.0370	-0.044		-4.60	-0.563	0.0440	-0.049		-5.12	-0.759	0.0505	-0.062		-5.81	-3.412	0.3551	-0.128
	-4.63	-0.533	0.0397	-0.047		-4.89	-0.603	0.0470	-0.052		-5.41	-0.808	0.0534	-0.065		-6.10	-3.644	0.3790	-0.135
	-4.92	-0.571	0.0424	-0.050		-5.18	-0.643	0.0500	-0.055		-5.70	-0.857	0.0563	-0.068		-6.39	-3.876	0.4029	-0.142
	-5.21	-0.609	0.0451	-0.053		-5.47	-0.683	0.0530	-0.058		-6.00	-0.906	0.0592	-0.071		-6.68	-4.108	0.4268	-0.149
	-5.50	-0.647	0.0478	-0.056		-5.76	-0.723	0.0560	-0.061		-6.29	-0.955	0.0621	-0.074		-6.97	-4.340	0.4507	-0.156
	-5.79	-0.685	0.0505	-0.059		-6.05	-0.763	0.0590	-0.064		-6.58	-1.004	0.0650	-0.077		-7.26	-4.572	0.4746	-0.163
	-6.08	-0.723	0.0532	-0.062		-6.34	-0.803	0.0620	-0.067		-6.87	-1.053	0.0679	-0.080		-7.55	-4.804	0.4985	-0.170
	-6.37	-0.761	0.0559	-0.065		-6.63	-0.843	0.0650	-0.070		-7.16	-1.102	0.0708	-0.083		-7.84	-5.036	0.5224	-0.177
	-6.66	-0.799	0.0586	-0.068		-6.92	-0.883	0.0680	-0.073		-7.45	-1.151	0.0737	-0.086		-8.13	-5.268	0.5463	-0.184
	-6.95	-0.837	0.0613	-0.071		-7.21	-0.923	0.0710	-0.076		-7.74	-1.200	0.0766	-0.089		-8.42	-5.500	0.5702	-0.191
	-7.24	-0.875	0.0640	-0.074		-7.50	-0.963	0.0740	-0.079		-8.03	-1.249	0.0795	-0.092		-8.72	-5.732	0.5941	-0.198
	-7.53	-0.913	0.0667	-0.077		-7.79	-1.003	0.0770	-0.082		-8.32	-1.298	0.0824	-0.095		-9.01	-5.964	0.6180	-0.205
	-7.82	-0.951	0.0694	-0.080		-8.08	-1.043	0.0800	-0.085		-8.61	-1.347	0.0853	-0.098		-9.30	-6.196	0.6419	-0.212
	-8.11	-0.989	0.0721	-0.083		-8.37	-1.083	0.0830	-0.088		-8.90	-1.396	0.0882	-0.101		-9.59	-6.428	0.6658	-0.219
	-8.40	-1.027	0.0748	-0.086		-8.66	-1.123	0.0860	-0.091		-9.19	-1.445	0.0911	-0.104		-9.88	-6.660	0.6897	-0.226
	-8.69	-1.065	0.0775	-0.089		-8.95	-1.163	0.0890	-0.094		-9.48	-1.494	0.0940	-0.107		-10.17	-6.892	0.7136	-0.233
	-8.98	-1.103	0.0802	-0.092		-9.24	-1.203	0.0920	-0.097		-9.77	-1.543	0.0969	-0.110		-10.46	-7.124	0.7375	-0.240
	-9.27	-1.141	0.0829	-0.095		-9.53	-1.243	0.0950	-0.100		-10.06	-1.592	0.0998	-0.113		-10.75	-7.356	0.7614	-0.247
	-9.56	-1.179	0.0856	-0.098		-9.82	-1.283	0.0980	-0.103		-10.35	-1.641	0.1027	-0.116		-11.04	-7.588	0.7853	-0.254
	-9.85	-1.217	0.0883	-0.101		-10.11	-1.323	0.1010	-0.106		-10.64	-1.690	0.1056	-0.119		-11.33	-7.820	0.8092	-0.261
	-10.14	-1.255	0.0910	-0.104		-10.40	-1.363	0.1040	-0.109		-10.93	-1.739	0.1085	-0.122		-11.62	-8.052	0.8331	-0.268
	-10.43	-1.293	0.0937	-0.107		-10.69	-1.403	0.1070	-0.112		-11.22	-1.788	0.1114	-0.125		-11.91	-8.284	0.8570	-0.275
	-10.72	-1.331	0.0964	-0.110		-10.98	-1.443	0.1100	-0.115		-11.51	-1.837	0.1143	-0.128		-12.20	-8.516	0.8809	-0.282
	-11.01	-1.369	0.0991	-0.113		-11.27	-1.483	0.1130	-0.118		-11.80	-1.886	0.1172	-0.131		-12.49	-8.748	0.9048	-0.289
	-11.30	-1.407	0.1018	-0.116		-11.56	-1.523	0.1160	-0.121		-12.09	-1.935	0.1201	-0.134		-12.78	-8.980	0.9287	-0.296
	-11.59	-1.445	0.1045	-0.119		-11.85	-1.563	0.1190	-0.124		-12.38	-1.984	0.1230	-0.137		-13.07	-9.212	0.9526	-0.303
	-11.88	-1.483	0.1072	-0.122		-12.14	-1.603	0.1220	-0.127		-12.67	-2.033	0.1259	-0.140		-13.36	-9.444	0.9765	-0.310
	-12.17	-1.521	0.1099	-0.125		-12.43	-1.643	0.1250	-0.130		-12.96	-2.082	0.1288	-0.143		-13.65	-9.676	1.0004	-0.317
	-12.46	-1.559	0.1126	-0.128		-12.72	-1.683	0.1280	-0.133		-13.25	-2.131	0.1317	-0.146		-13.94	-9.908	1.0243	-0.324
	-12.75	-1.597	0.1153	-0.131		-13.01	-1.723	0.1310	-0.136		-13.54	-2.180	0.1346	-0.149		-14.23	-10.140	1.0482	-0.331
	-13.04	-1.635	0.1180	-0.134		-13.30	-1.763	0.1340	-0.139		-13.83	-2.229	0.1375	-0.152		-14.52	-10.372	1.0721	-0.338
	-13.33	-1.673	0.1207	-0.137		-13.59	-1.803	0.1370	-0.142		-14.12	-2.278	0.1404	-0.155		-14.81	-10.604	1.0960	-0.345
	-13.62	-1.711	0.1234	-0.140		-13.88	-1.843	0.1400	-0.145		-14.41	-2.327	0.1433	-0.158		-15.10	-10.836	1.1199	-0.352
	-13.91	-1.749	0.1261	-0.143		-14.17	-1.883	0.1430	-0.148		-14.70	-2.376	0.1462	-0.161		-15.39	-11.068	1.1438	-0.359
	-14.20	-1.787	0.1288	-0.146		-14.46	-1.923	0.1460	-0.151		-15.00	-2.425	0.1491	-0.164		-15.68	-11.300	1.1677	-0.366
	-14.49	-1.825	0.1315	-0.149		-14.75	-1.963	0.1490	-0.154		-15.29	-2.474	0.1520	-0.167		-15.97	-11.532	1.1916	-0.373
	-14.78	-1.863	0.1342	-0.152		-15.04	-2.003	0.1520	-0.157		-15.58	-2.523	0.1549	-0.170		-16.26	-11.764	1.2155	-0.380
	-15.07	-1.901	0.1369	-0.155		-15.33	-2.043	0.1550	-0.160		-15.87	-2.572	0.1578	-0.173		-16.55	-11.996	1.2394	-0.387
	-15.36	-1.939	0.1396	-0.158		-15.62	-2.083	0.1580	-0.163		-16.16	-2.621	0.1607	-0.176		-16.84	-12.228	1.2633	-0.394
	-15.65	-1.977	0.1423	-0.161		-15.91	-2.123	0.1610	-0.166		-16.45	-2.670	0.1636	-0.179		-17.13	-12.460	1.2872	-0.401
	-15.94	-2.015	0.1450	-0.164		-16.20	-2.163	0.1640	-0.169		-16.74	-2.719	0.1665	-0.182		-17.42	-12.692	1.3111	-0.408
	-16.23	-2.053	0.1477	-0.167		-16.49	-2.203	0.1670	-0.172		-17.03	-2.768	0.1694	-0.185		-17.71	-12.924	1.3350	-0.415
	-16.52	-2.091	0.1504	-0.170		-16.78	-2.243	0.1700	-0.175		-17.32	-2.817	0.1723	-0.188		-18.00	-13.156	1.3589	-0.422
	-16.81	-2.129	0.1531	-0.173		-17.07	-2.283	0.1730	-0.178		-17.61	-2.866	0.1752	-0.191		-18.29	-13.388	1.3828	-0.429
	-17.10	-2.167	0.1558	-0.176		-17.36	-2.323	0.1760	-0.181		-17.90	-2.915	0.1781	-0.194		-18.58	-13.620	1.4067	-0.436
	-17.39	-2.205	0.1585	-0.179		-17.65	-2.363	0.1790	-0.184		-18.19	-2.964	0.1810	-0.197		-18.87	-13.852	1.4306	-0.443
	-17.68	-2.243	0.1612	-0.182		-17.94	-2.403	0.1820	-0.187		-18.48	-3.013	0.1839	-0.200		-19.16	-14.084	1.4545	-0.450
	-17.97	-2.281	0.1639	-0.185		-18.23	-2.443	0.1850	-0.190		-18.77	-3.062	0.1868	-0.203		-19.45	-14.316	1.4784	-0.457
	-18.26	-2.319	0.1666	-0.188		-18.52	-2.483	0.1880	-0.193		-19.06	-3.111	0.1897	-0.206		-19.74	-14.548	1.5023	-0.464
	-18.55	-2.357	0.1693	-0.191		-18.81	-2.523	0.1910	-0.196		-19.35	-3.160	0.1926	-0.209		-20.03	-14.780	1.5262	-

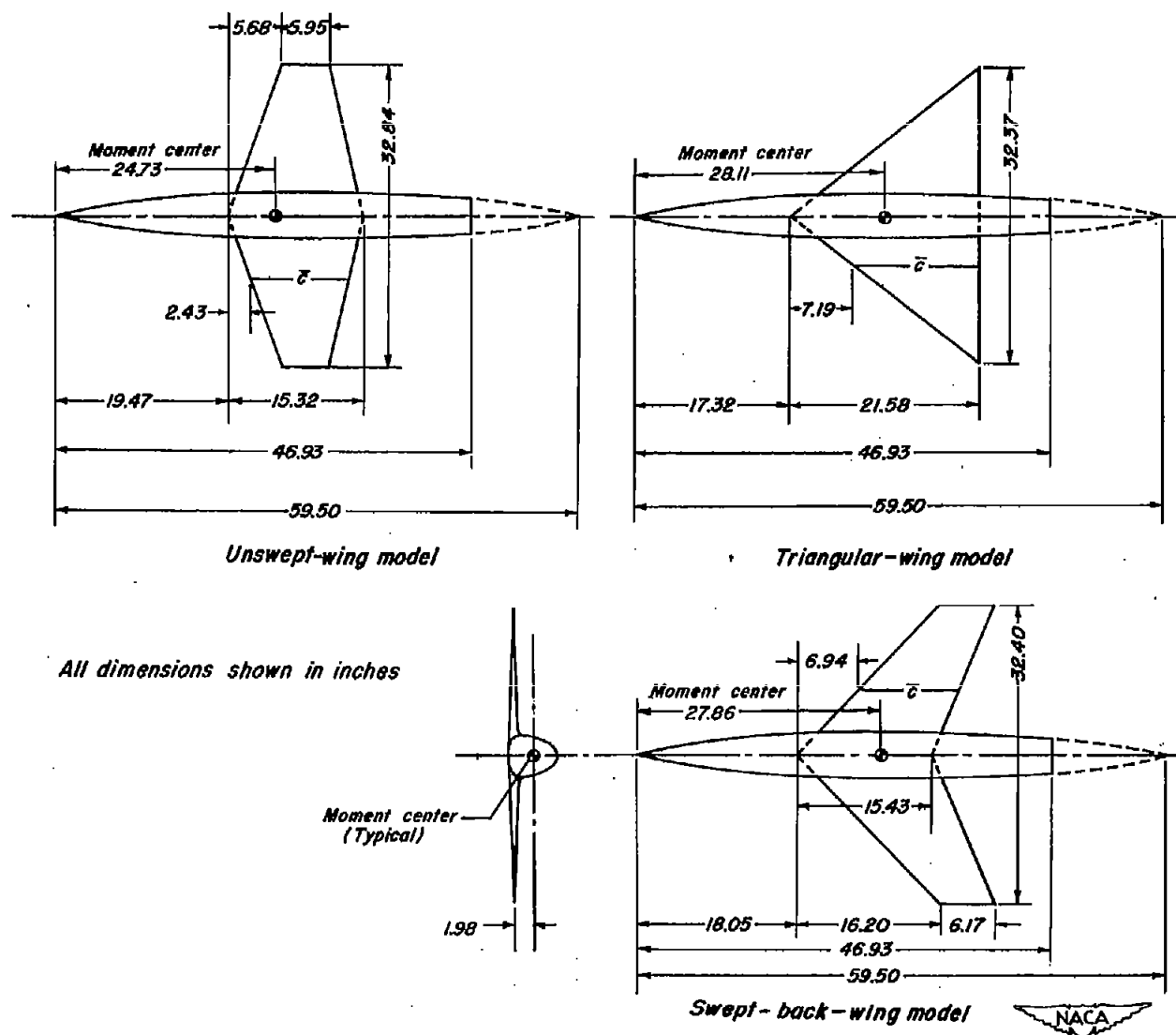


Figure 1.—Plan views and a typical front view of the models.

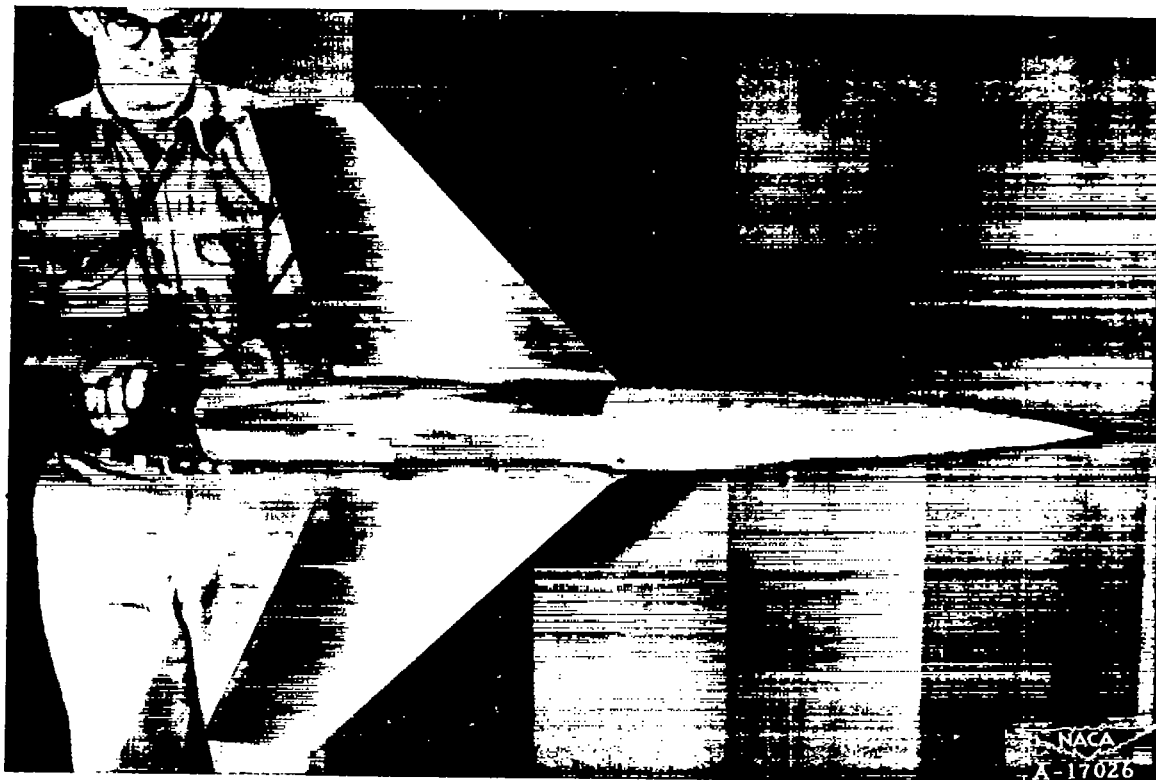
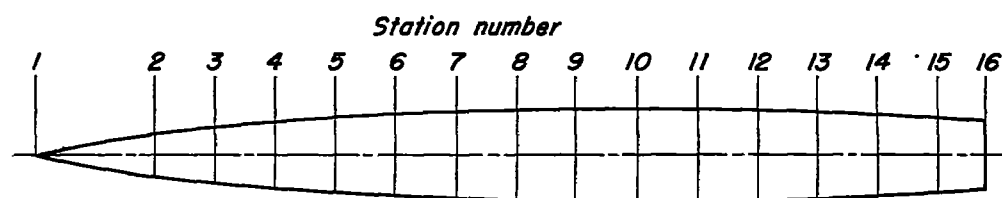
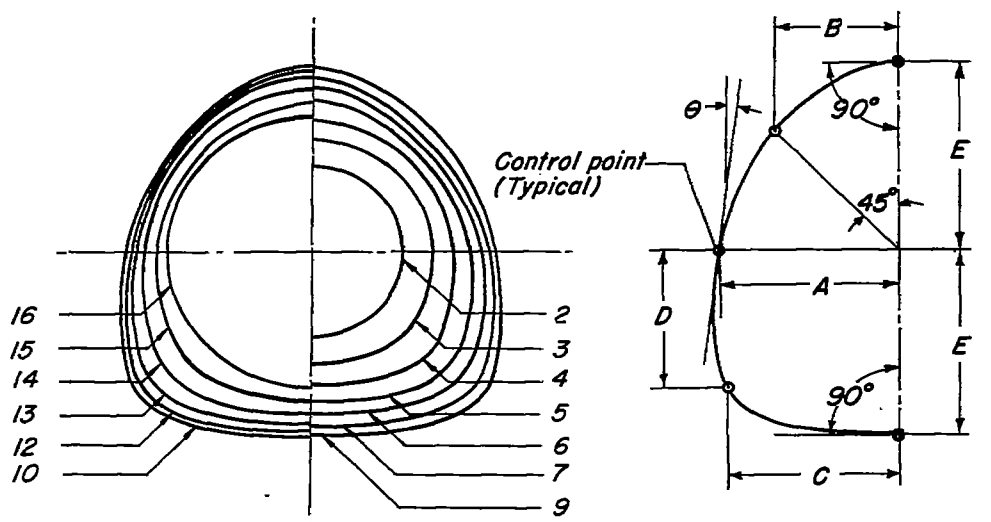


Figure 2.— Photograph of the swept-back wing model.



(a) Side view of body.



(b) Various sections of body

(c) Typical non circular cross-section

Sta. No.	Body Sta.	A	B	C	D	E	θ
1	0	-	-	-	-	-	-
2	5.950	Circular in shape, $r = 1.106$					
3	8.925	1.44	1.03	1.11	1.07	1.436	10°-28'
4	11.900	1.69	1.17	1.39	1.29	1.703	20°-48'
5	14.875	1.89	1.26	1.60	1.48	1.918	40°-12'
6	17.850	2.03	1.34	1.77	1.63	2.088	50°-36'
7	20.825	2.12	1.42	1.91	1.73	2.215	70°
8	23.800	2.17	1.47	2.02	1.77	2.308	70°
9	26.775	2.21	1.51	2.08	1.77	2.362	70°
10	29.750	2.23	1.52	2.11	1.78	2.380	70°
11	32.725	2.20	1.51	2.09	1.77	2.362	70°
12	35.700	2.17	1.49	2.03	1.74	2.308	70°
13	38.675	2.11	1.46	1.90	1.69	2.215	70°
14	41.650	2.00	1.40	1.69	1.59	2.088	40°-40'
15	44.625	1.87	1.32	1.45	1.43	1.918	20°-20'
16	46.933	Circular in shape, $r = 1.750$					

All dimensions shown
in inches unless
otherwise noted.



(d) Table listing the location of control points.

Figure 3.-Geometric characteristics of the body of the present investigation.

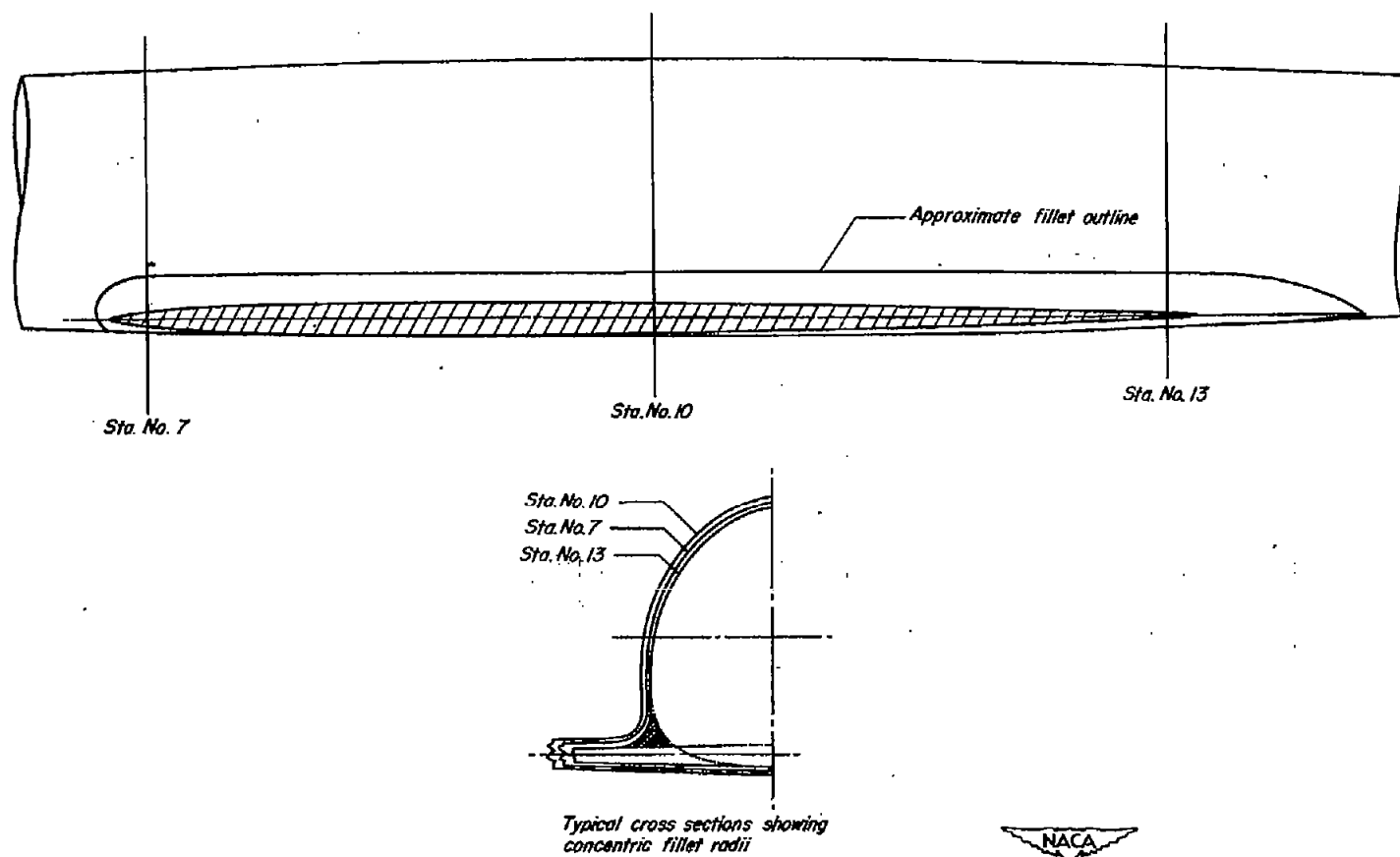
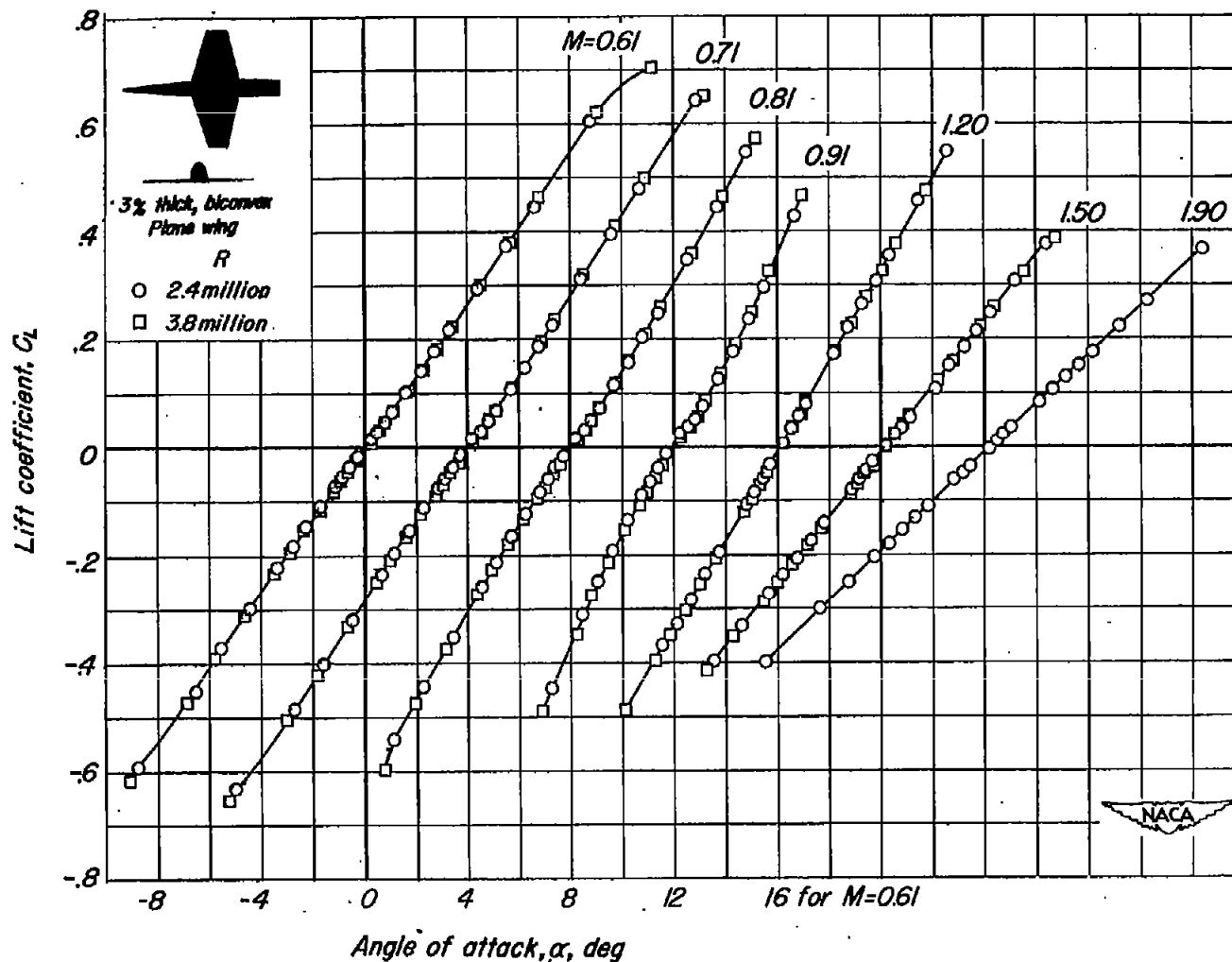


Figure 4.—Sections of the triangular-wing model showing the type of fillet.



(a) C_L vs α

Figure 5.-The variation of the aerodynamic characteristics of the unswept-wing model with lift coefficient at various Mach numbers.

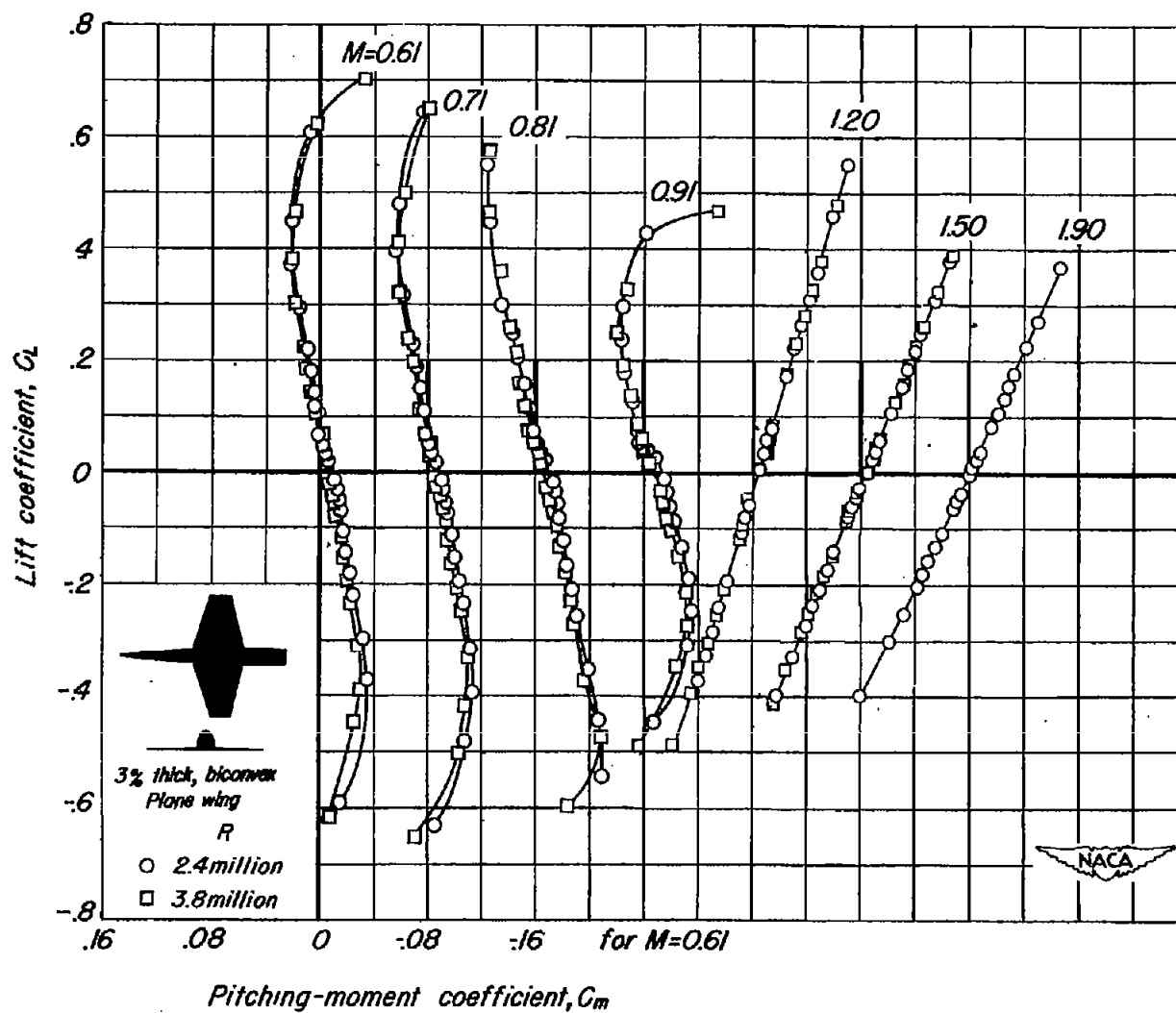
(b) C_L vs C_m

Figure 5.-Continued.

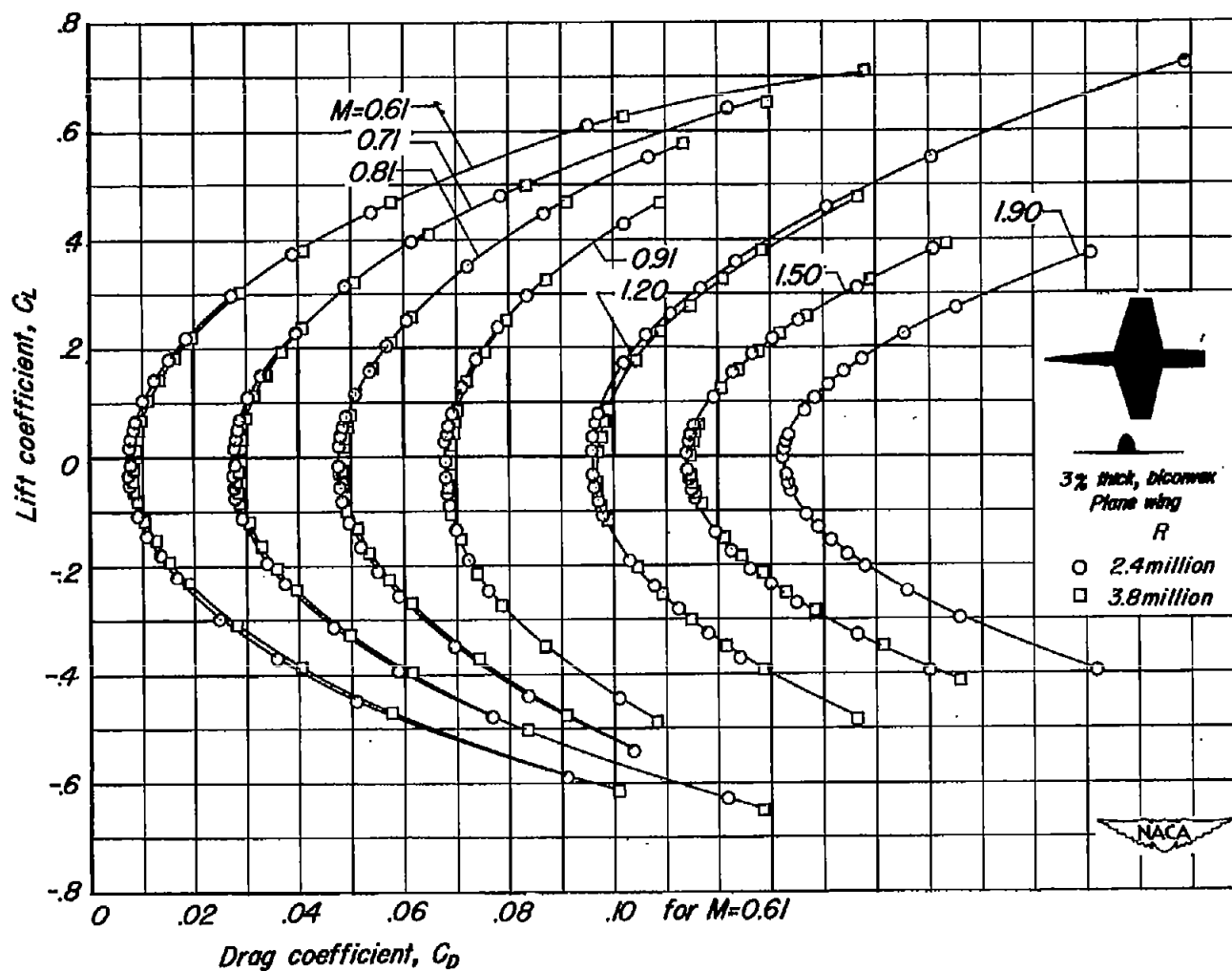
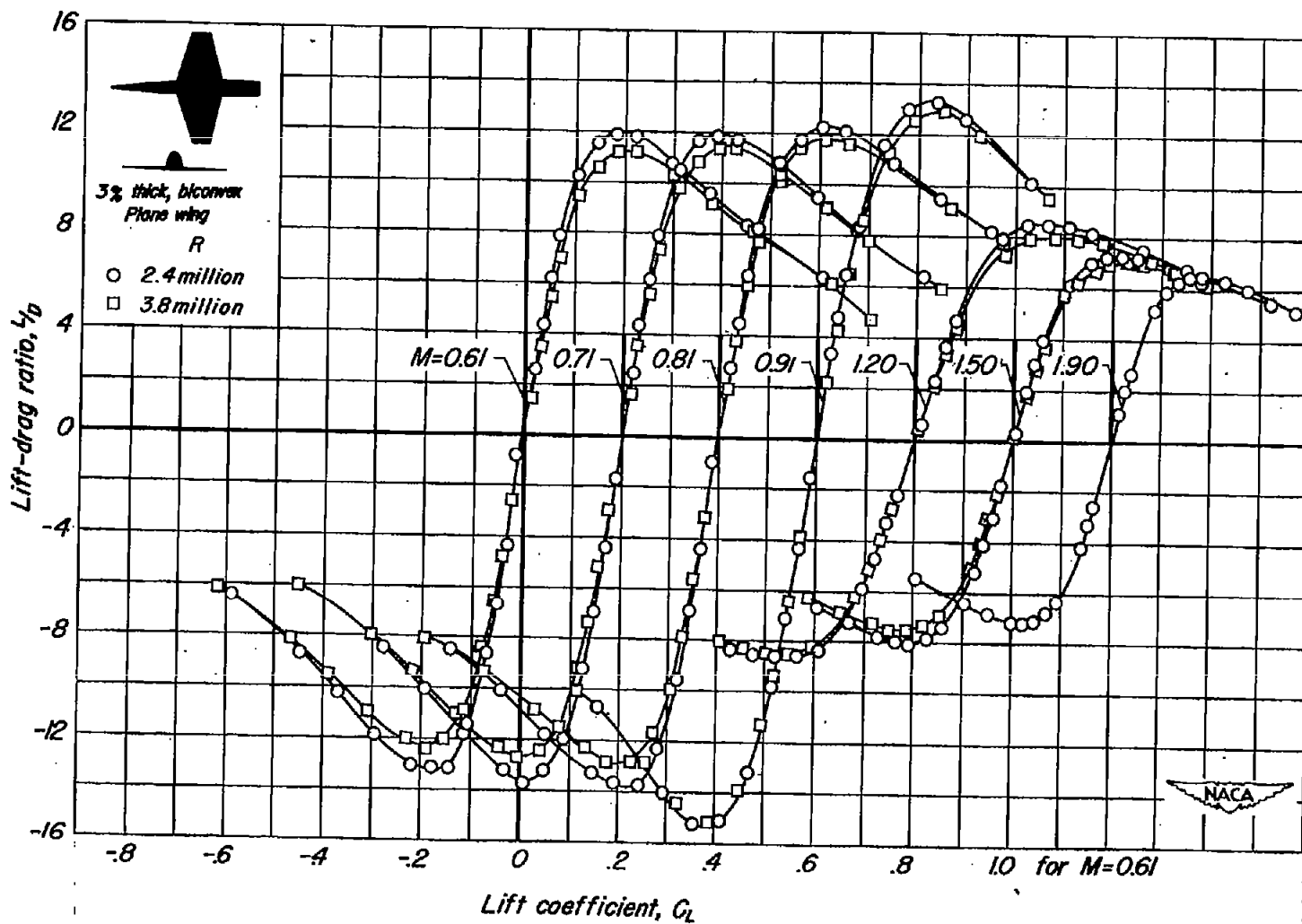
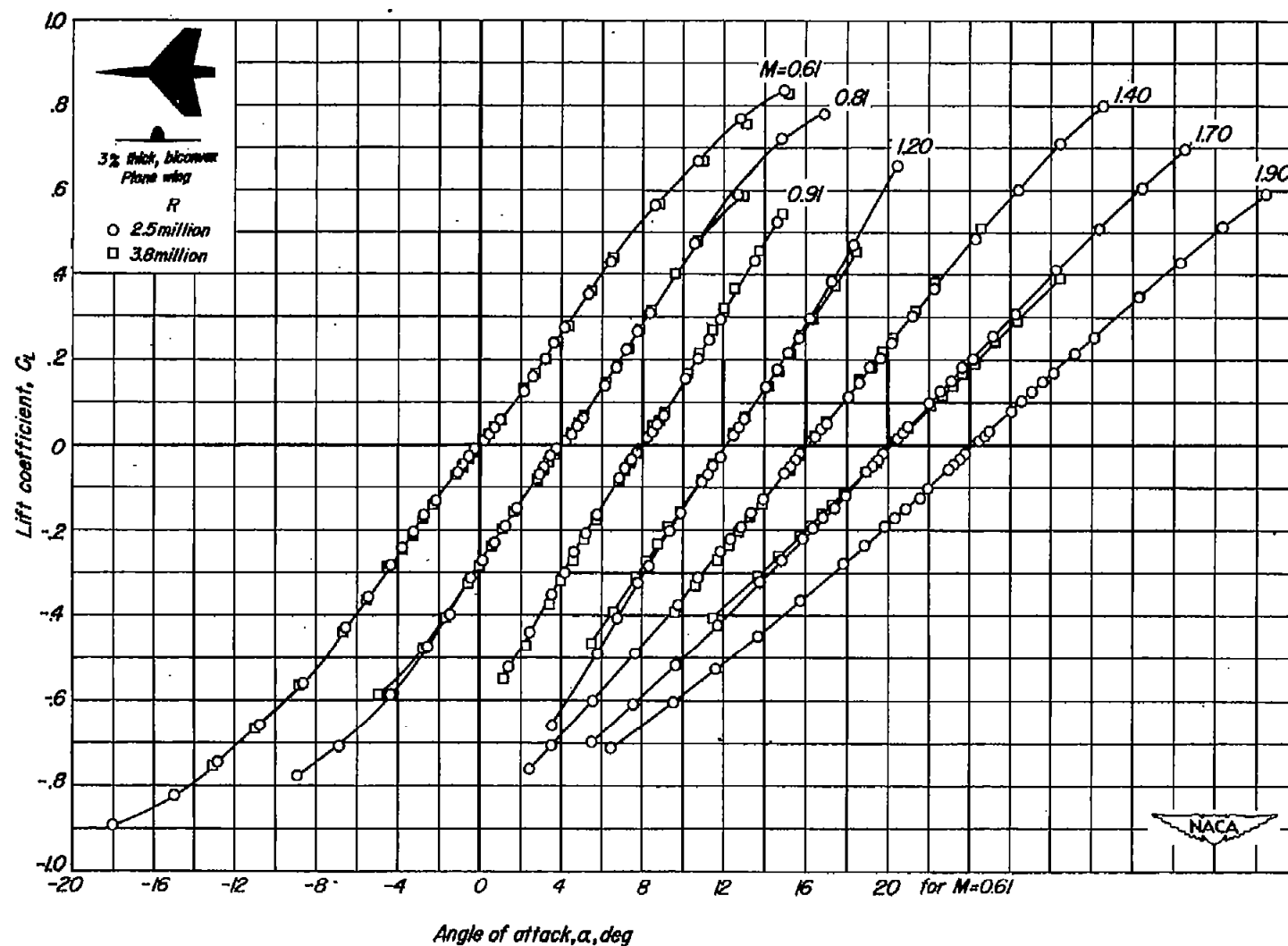
(c) C_L vs C_D

Figure 5.-Continued.



(d) L/D vs C_L

Figure 5.-Concluded.



(a) C_L vs α

Figure 6.-The variation of the aerodynamic characteristics of the swept-back-wing model with lift coefficient at various Mach numbers.

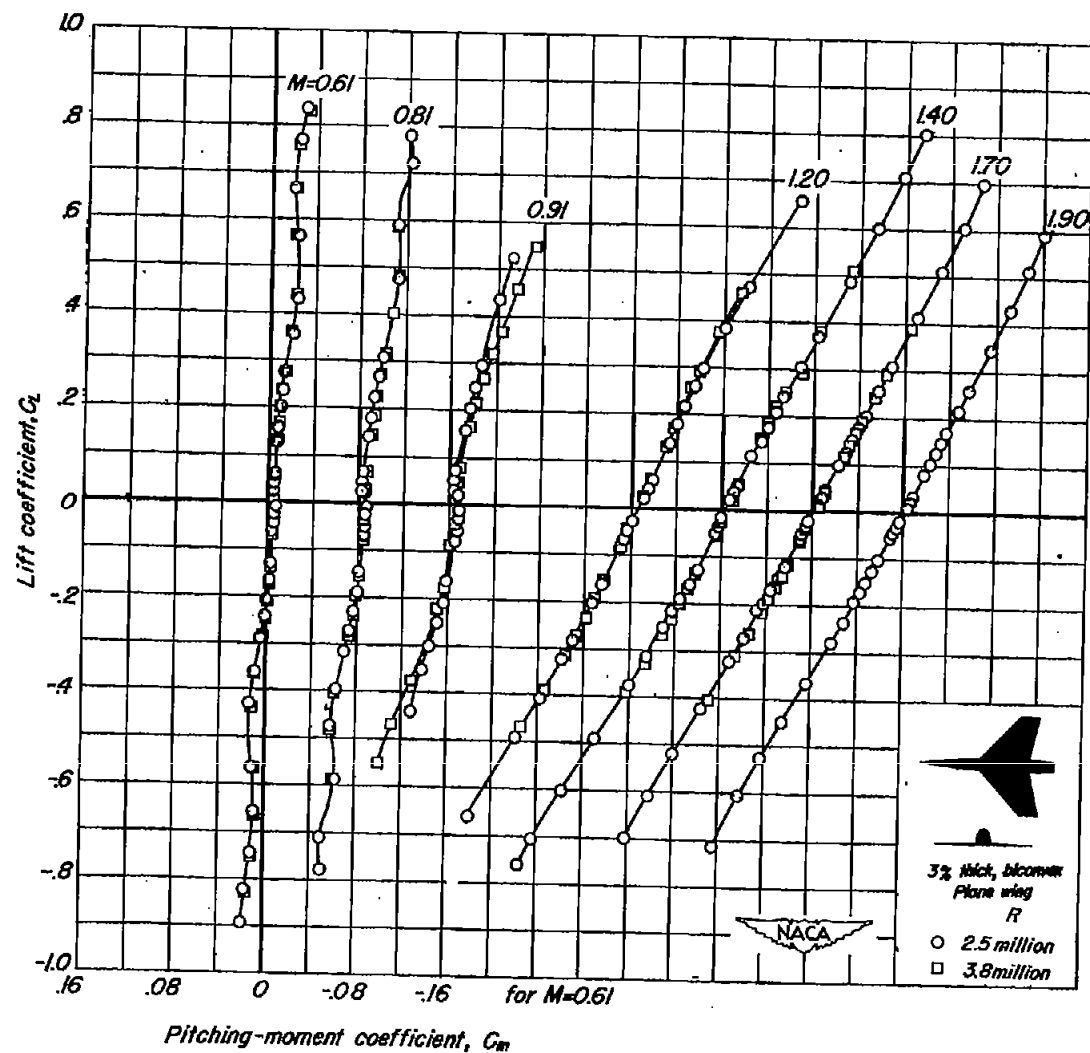
(b) C_L vs C_m

Figure 6.-Continued.

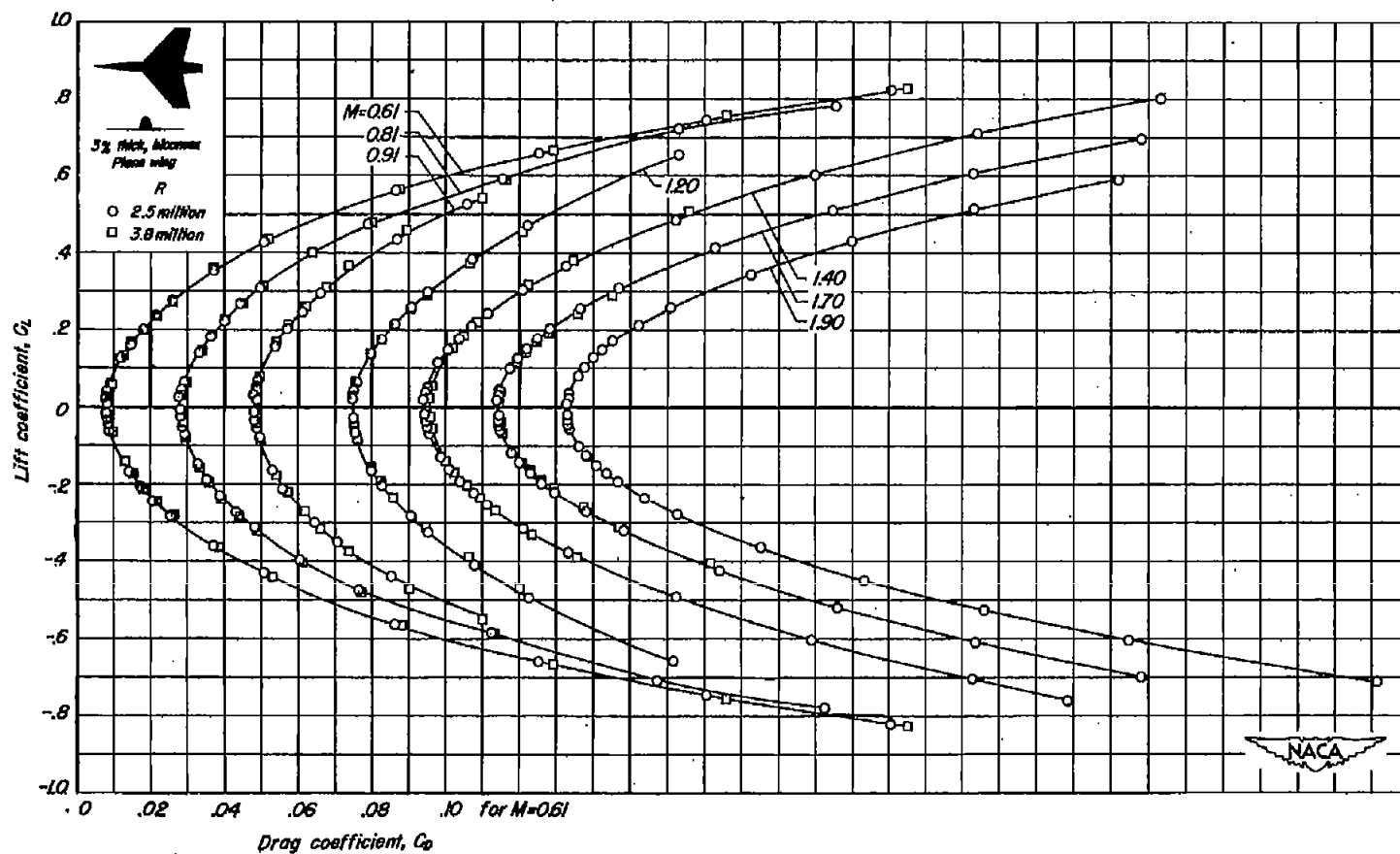
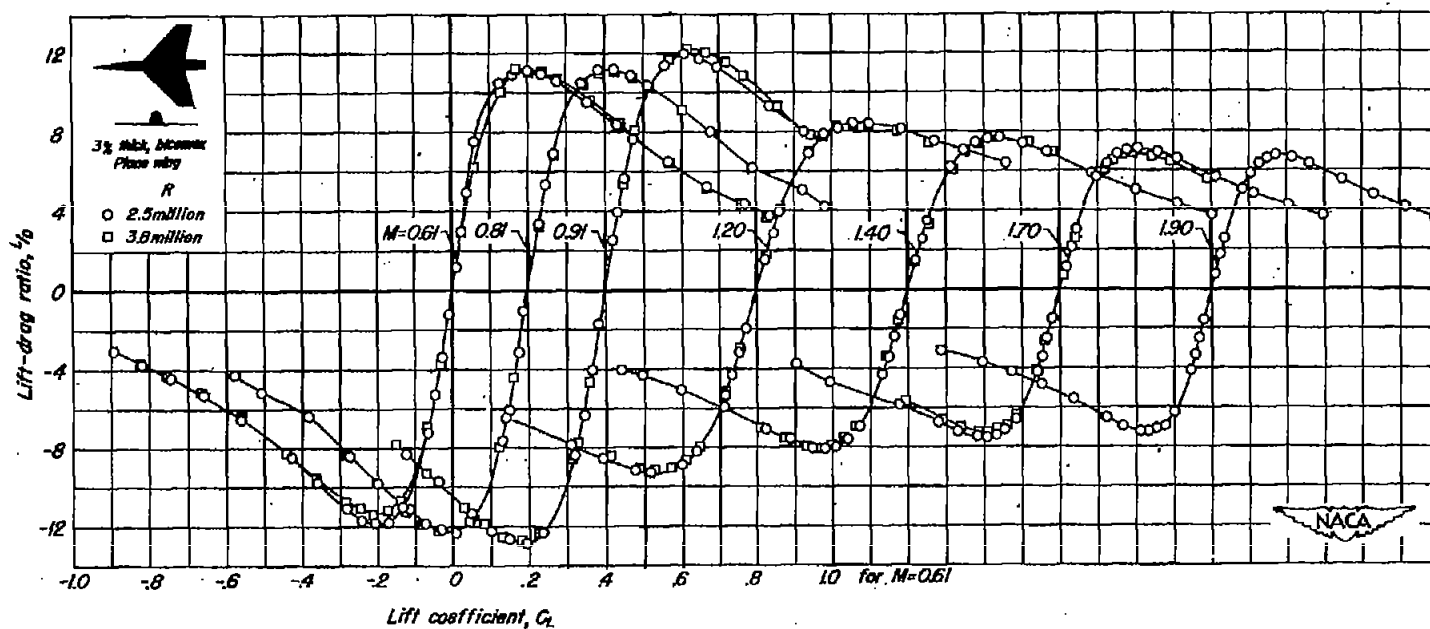
(c) C_L vs C_D

Figure 6-Continued.



(d) L/D vs C_L

Figure 6.-Concluded.

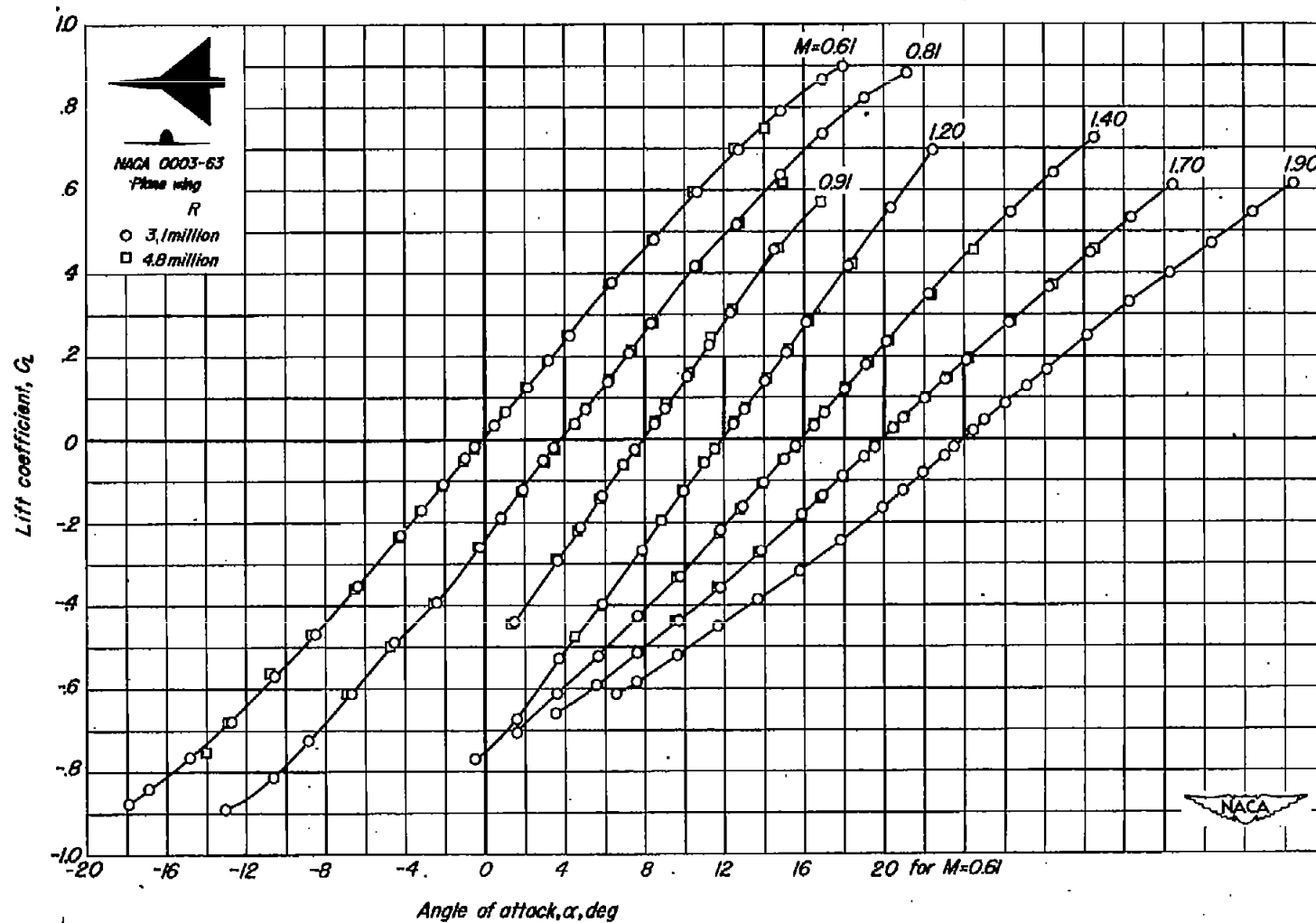


Figure 7.-The variation of the aerodynamic characteristics of the triangular wing model with lift coefficient at various Mach numbers.

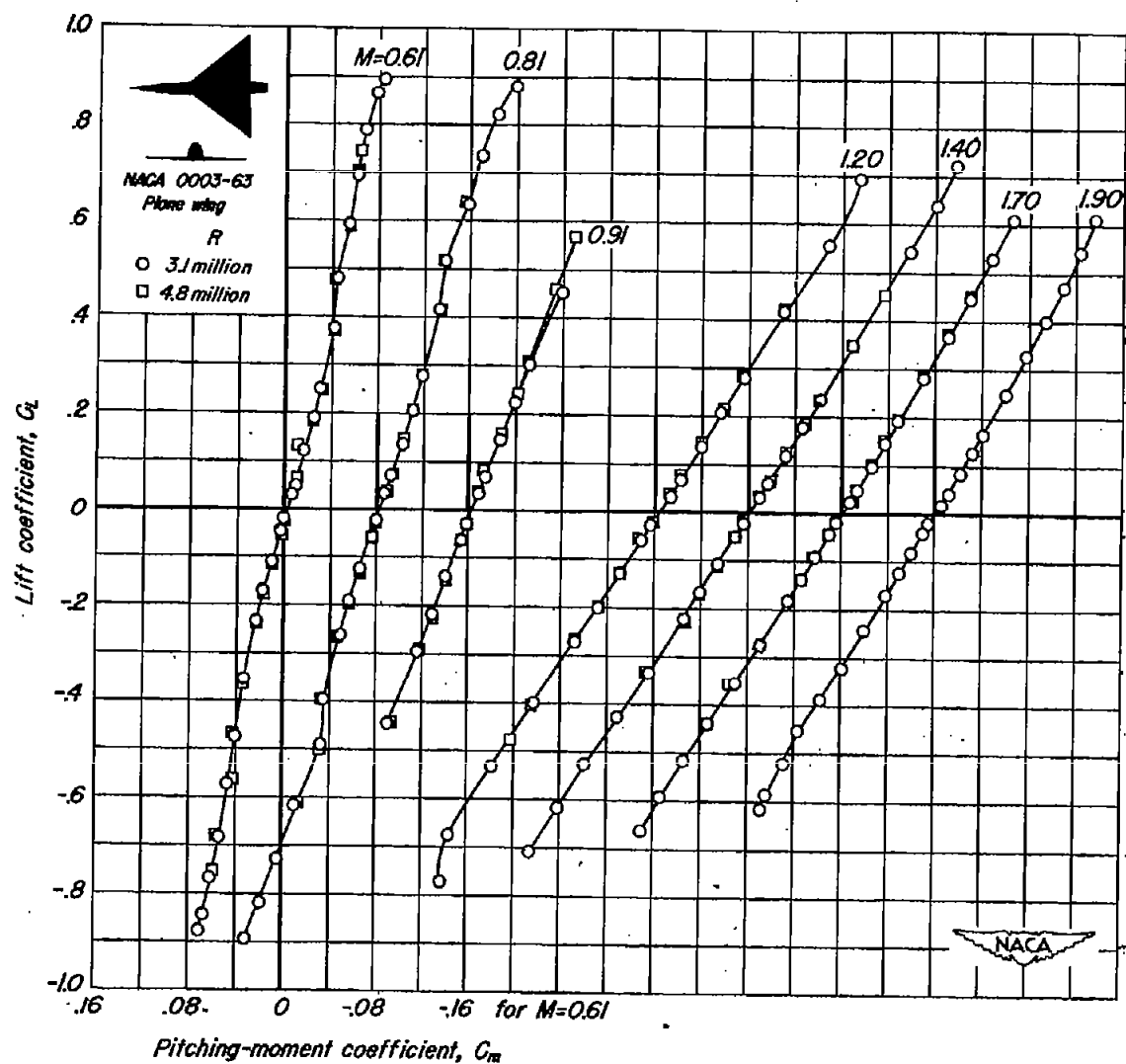
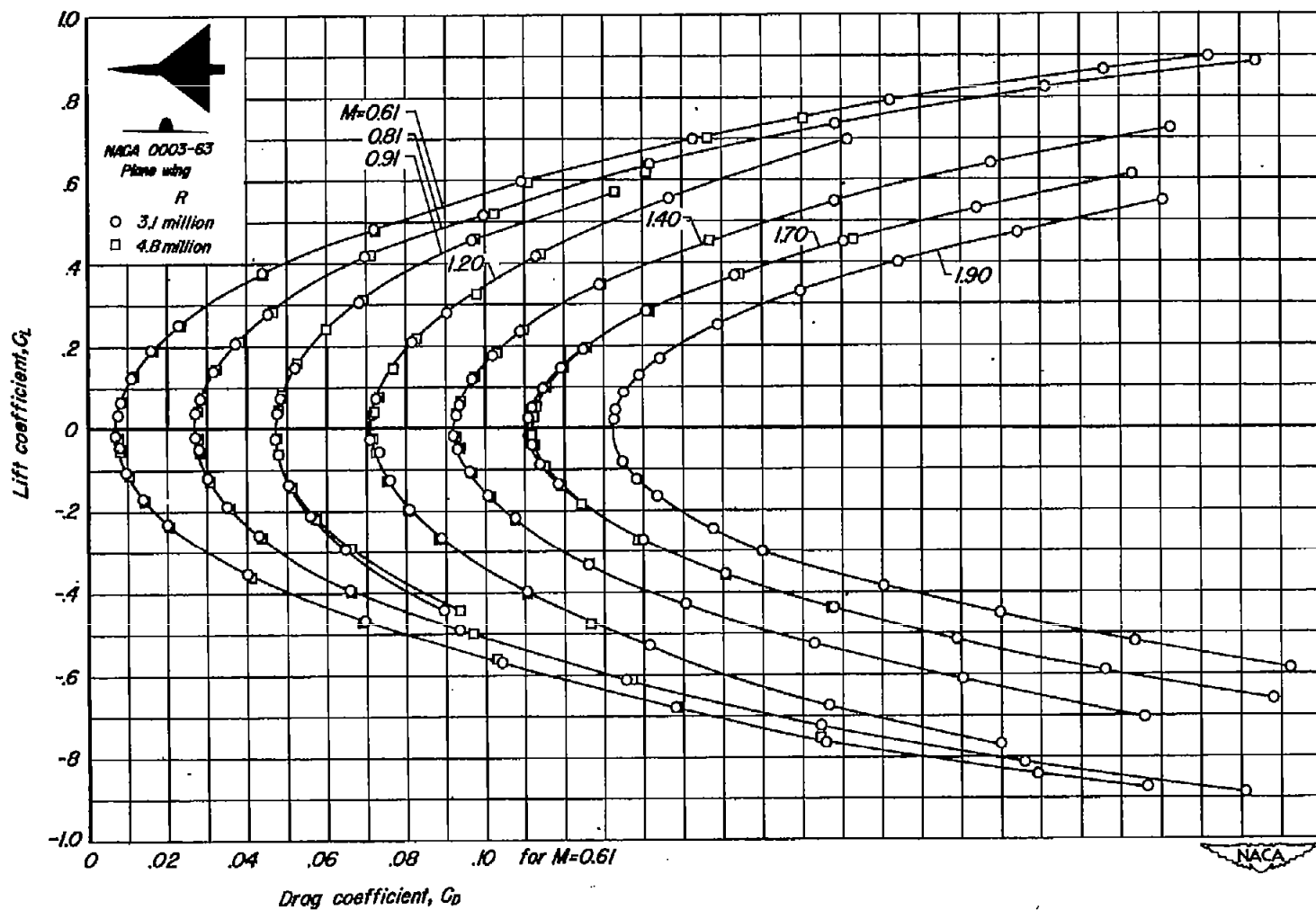
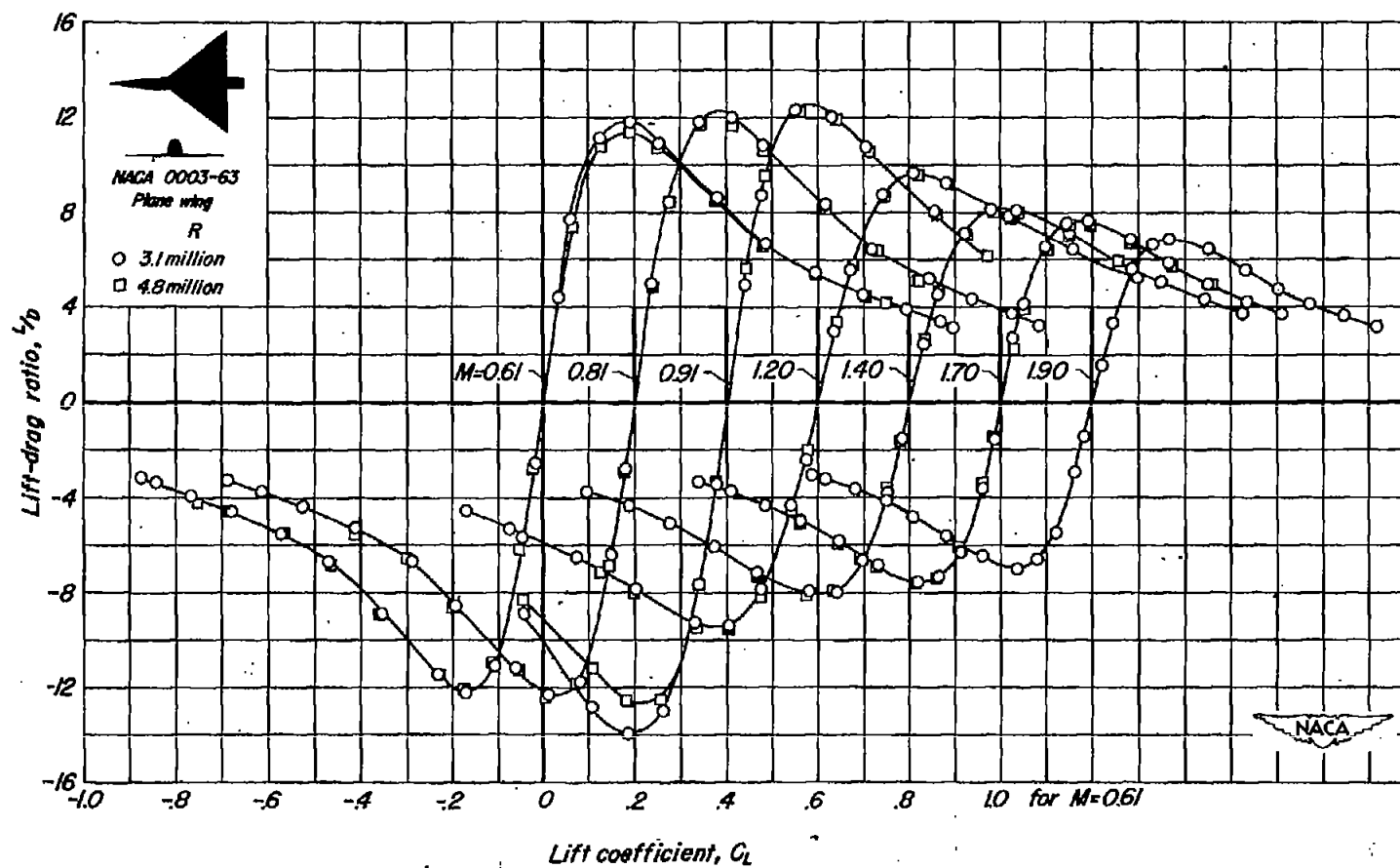
(b) C_L vs C_m

Figure 7.-Continued.



(c) C_L vs C_D

Figure 7.-Continued.



(d) L/D vs C_L

Figure 7.-Concluded.



(a) G_L vs α

Figure 8.-The variation of the aerodynamic characteristics with lift coefficient for three vertical positions of the unswept wing at various Mach numbers. Reynolds number, 3.8 million.

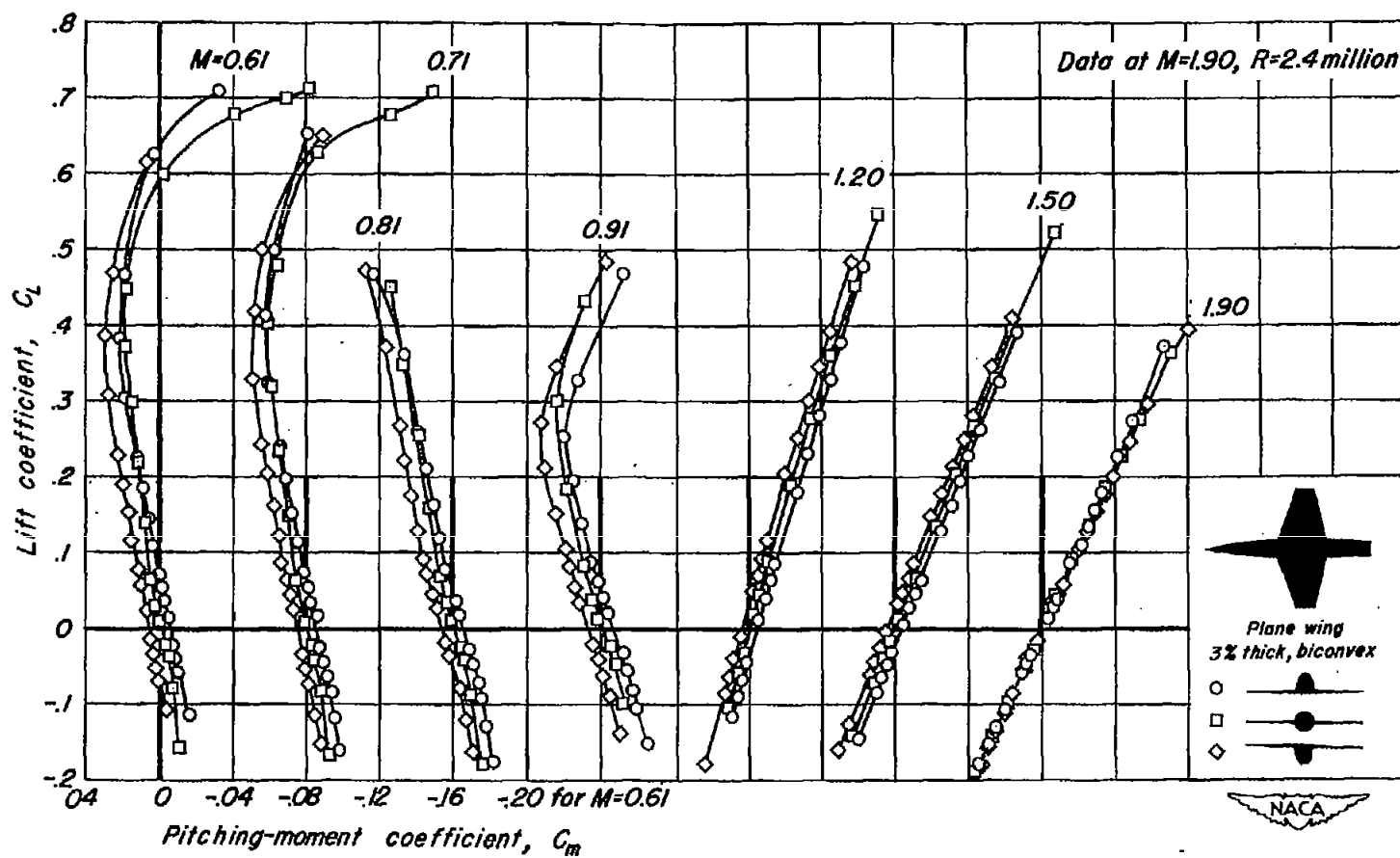
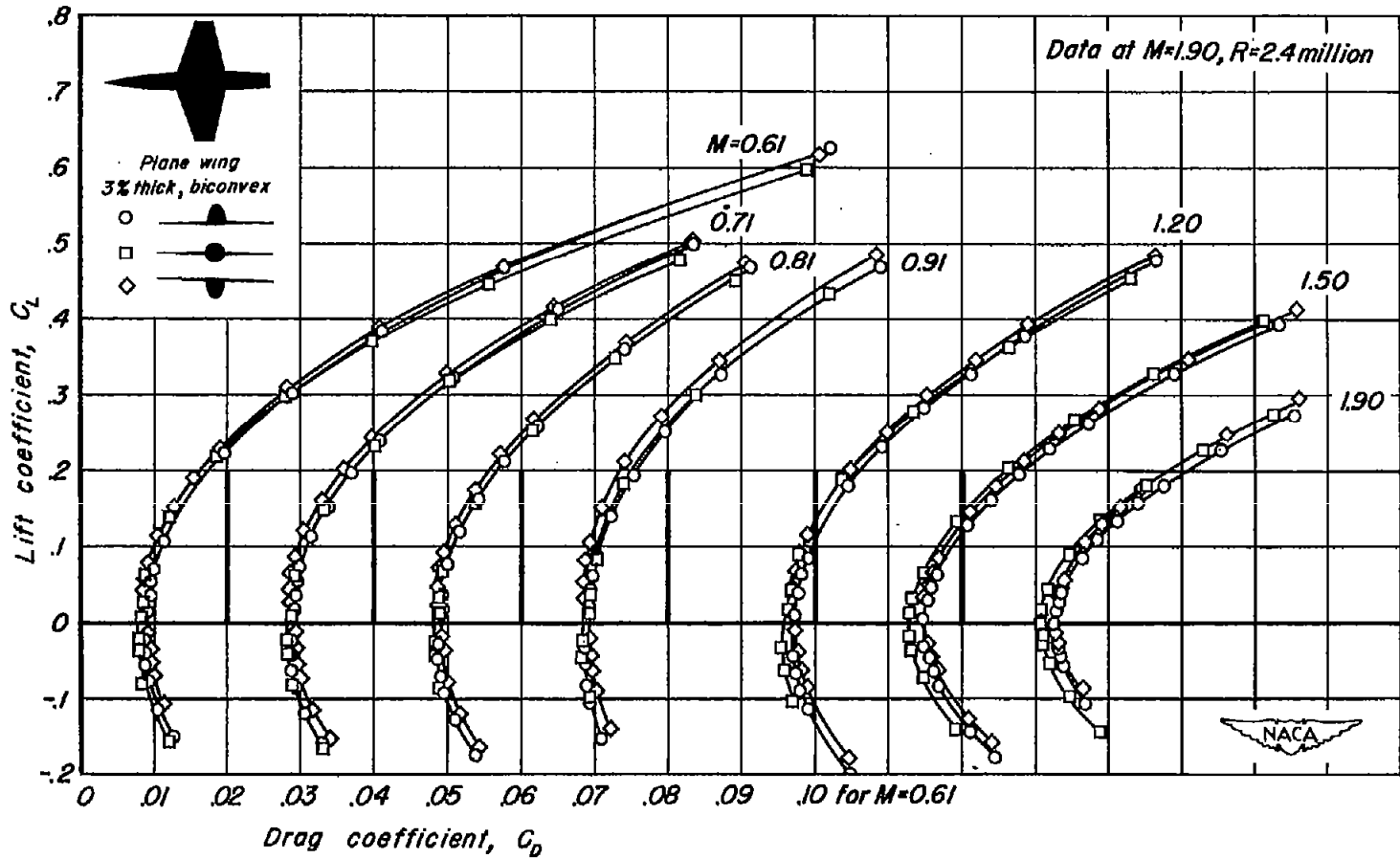
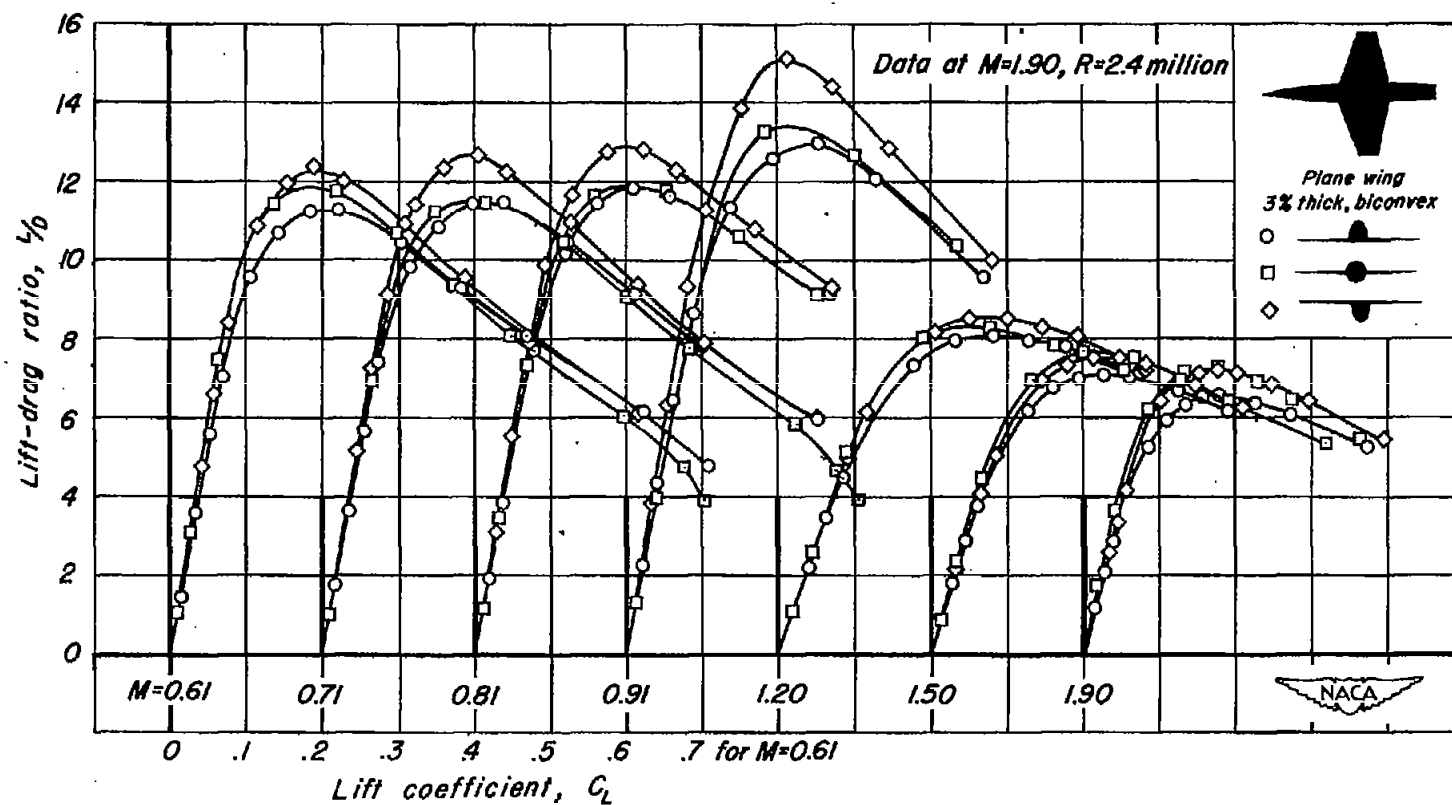
(b) C_L vs C_m

Figure 8.- Continued.



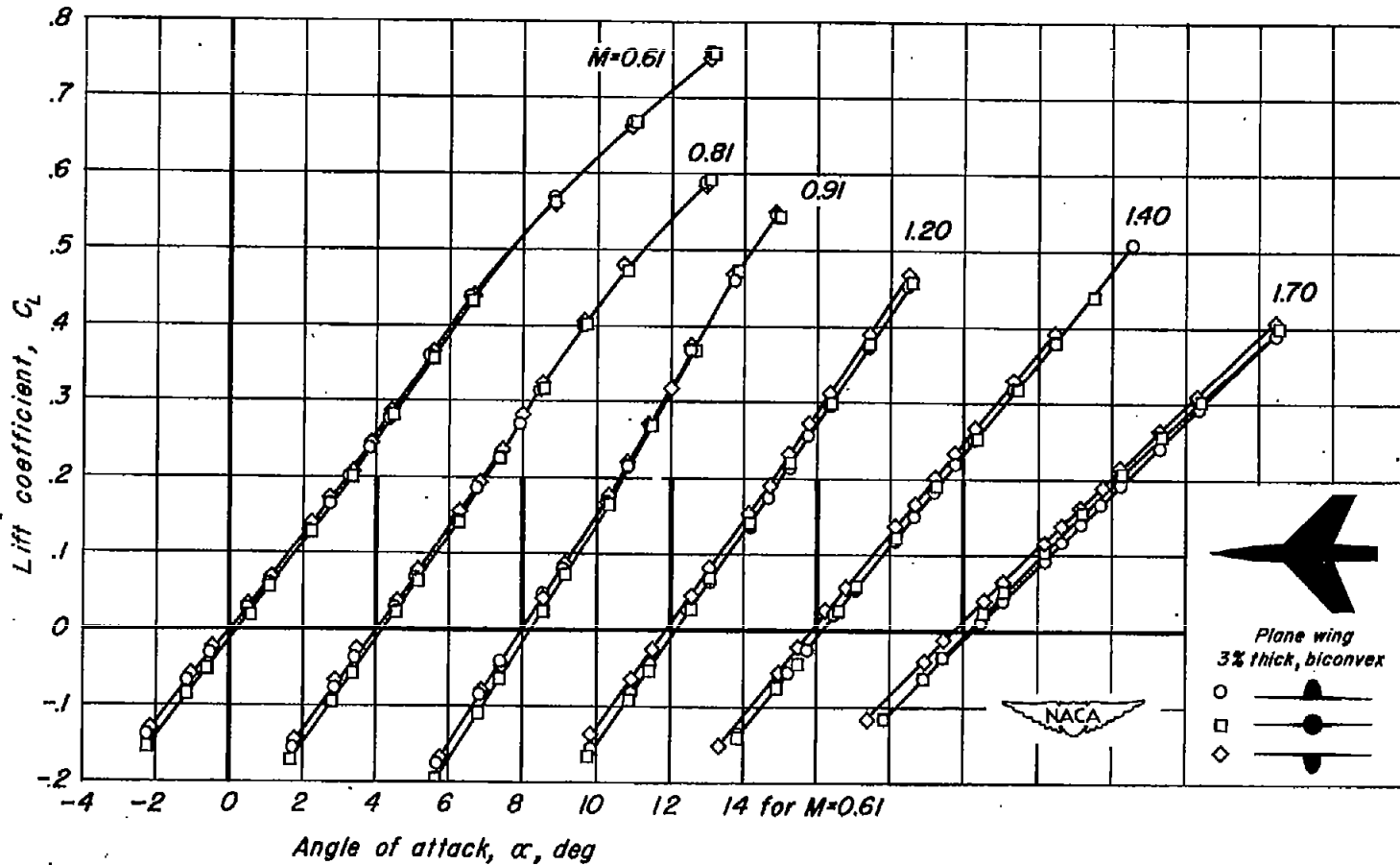
(c) C_L vs C_D

Figure 8.- Continued.



(d) L/D vs C_L

Figure 8.-Concluded.



(a) C_L vs α

Figure 9.-The variation of the aerodynamic characteristics with lift coefficient for three vertical positions of the swept-back wing at various Mach numbers. Reynolds number, 3.8 million.

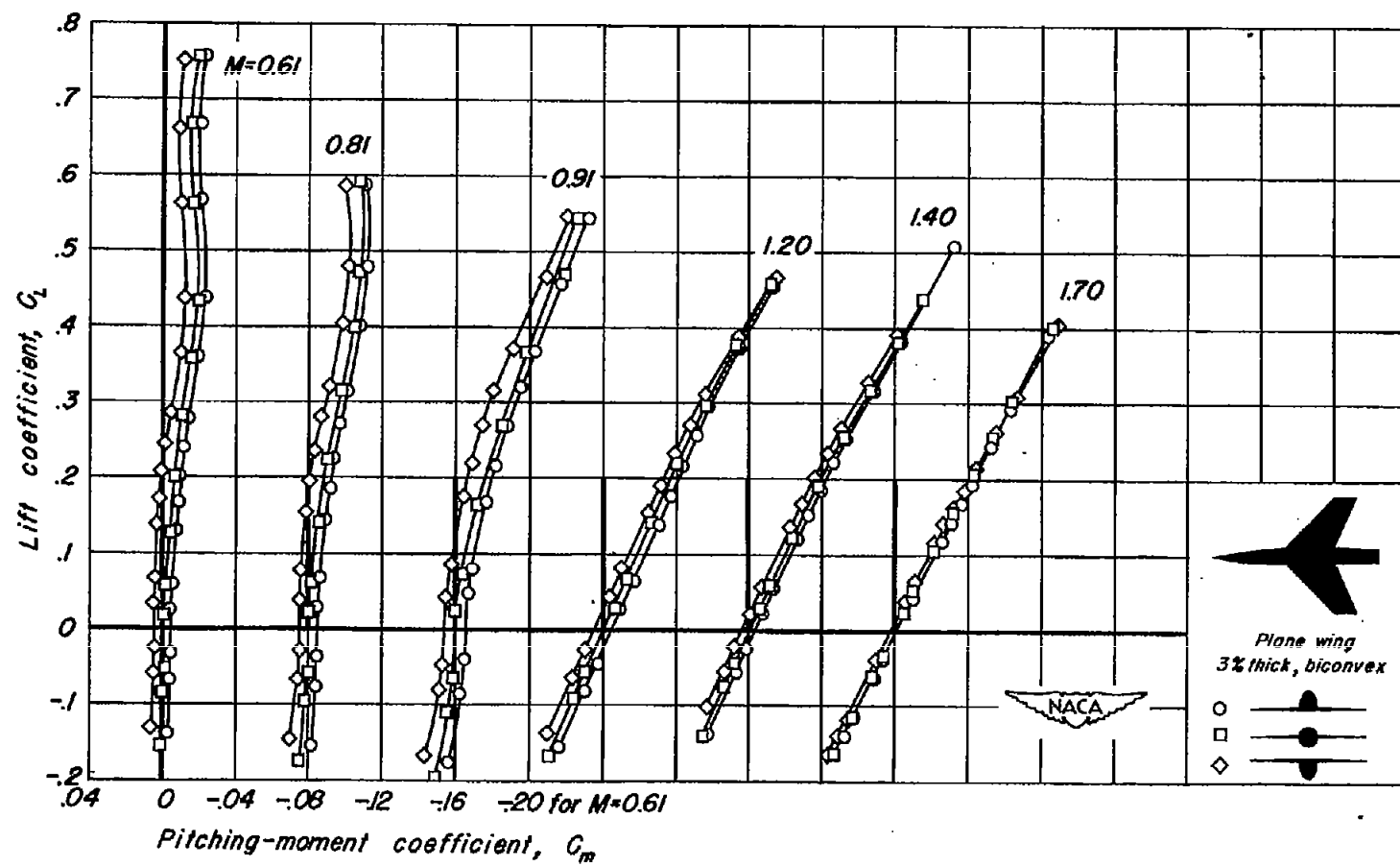
(b) C_L vs C_m

Figure 9.- Continued.

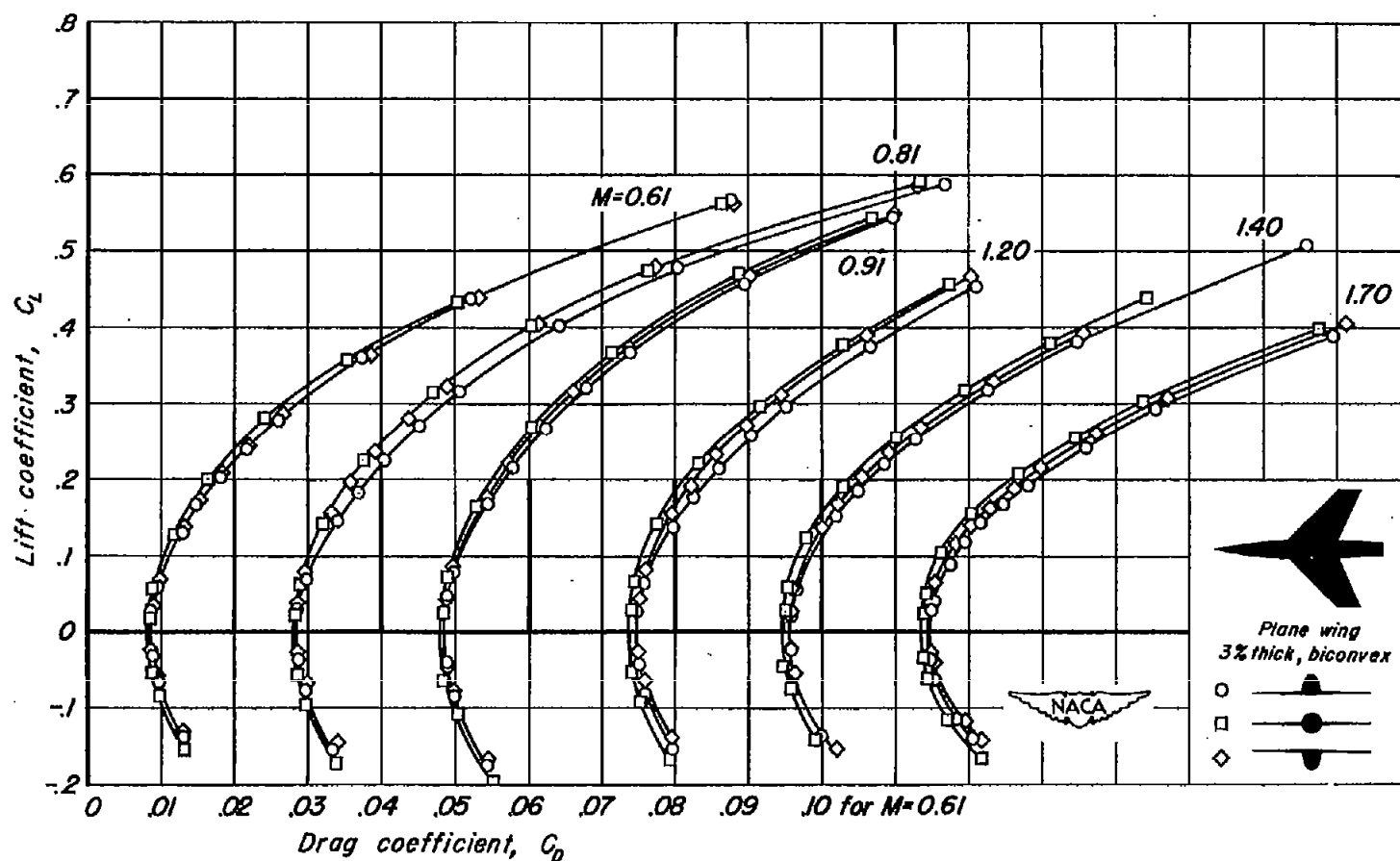
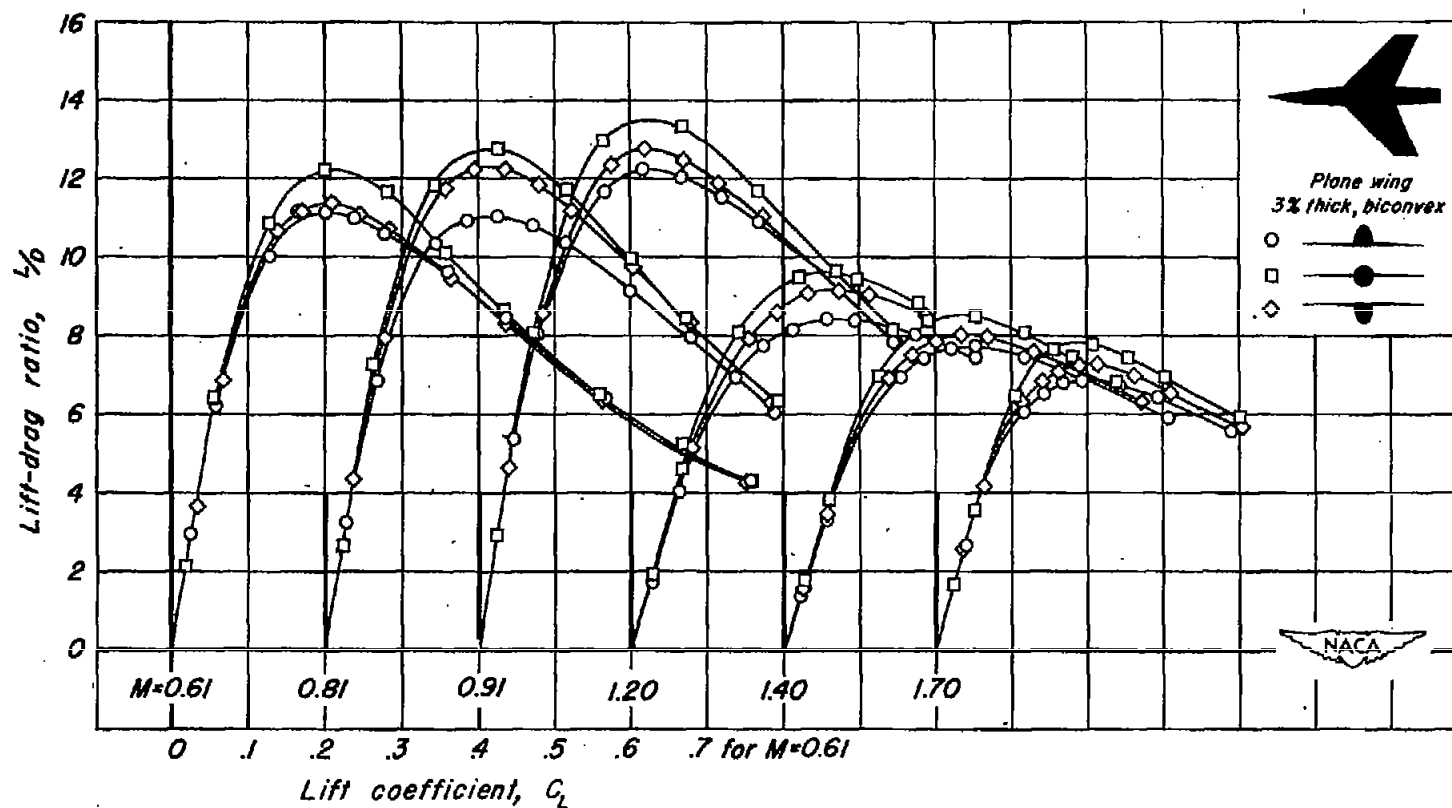
(c) C_L vs C_D

Figure 9.- Continued.



(d) L/D vs C_L

Figure 9.- Concluded.

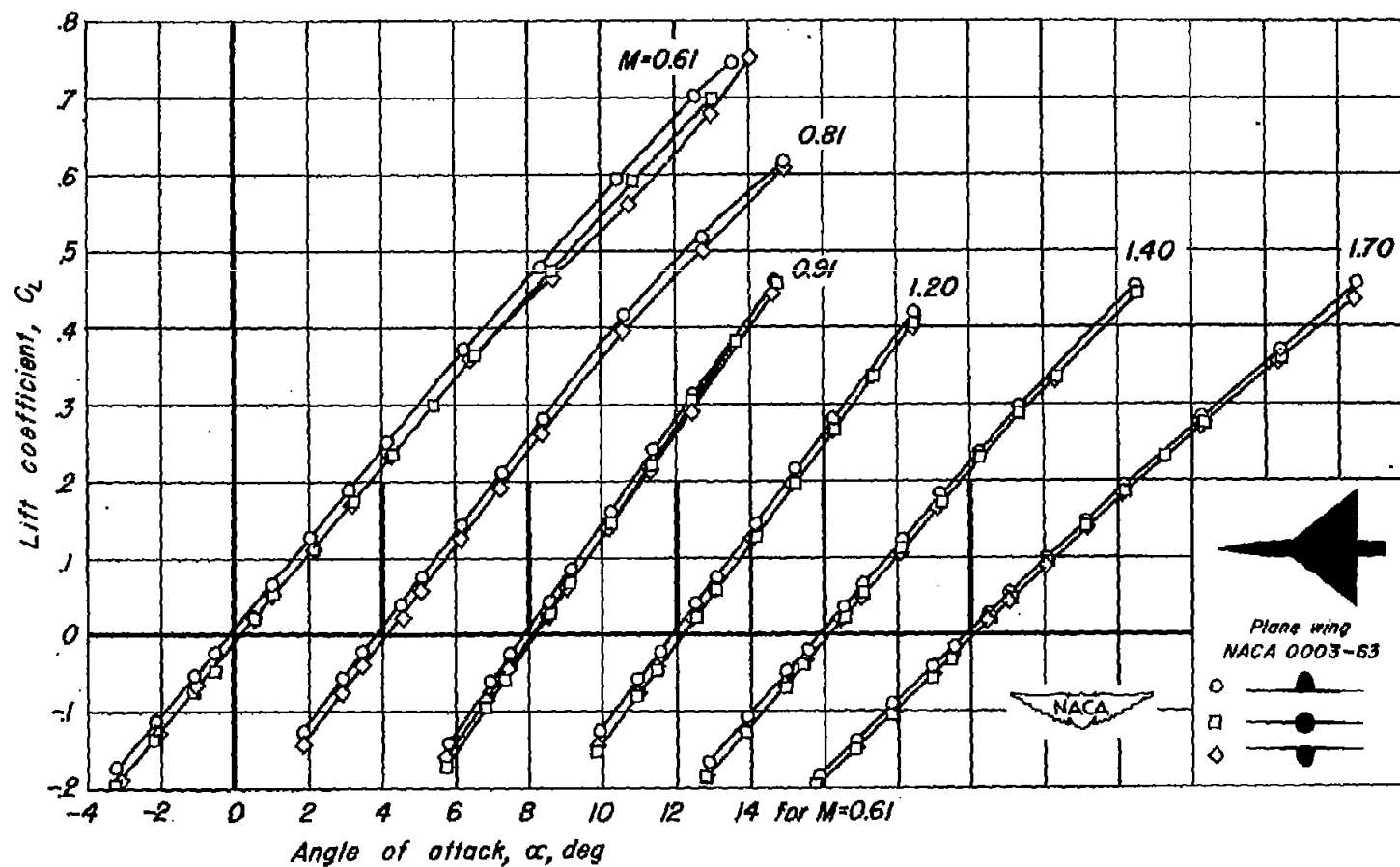
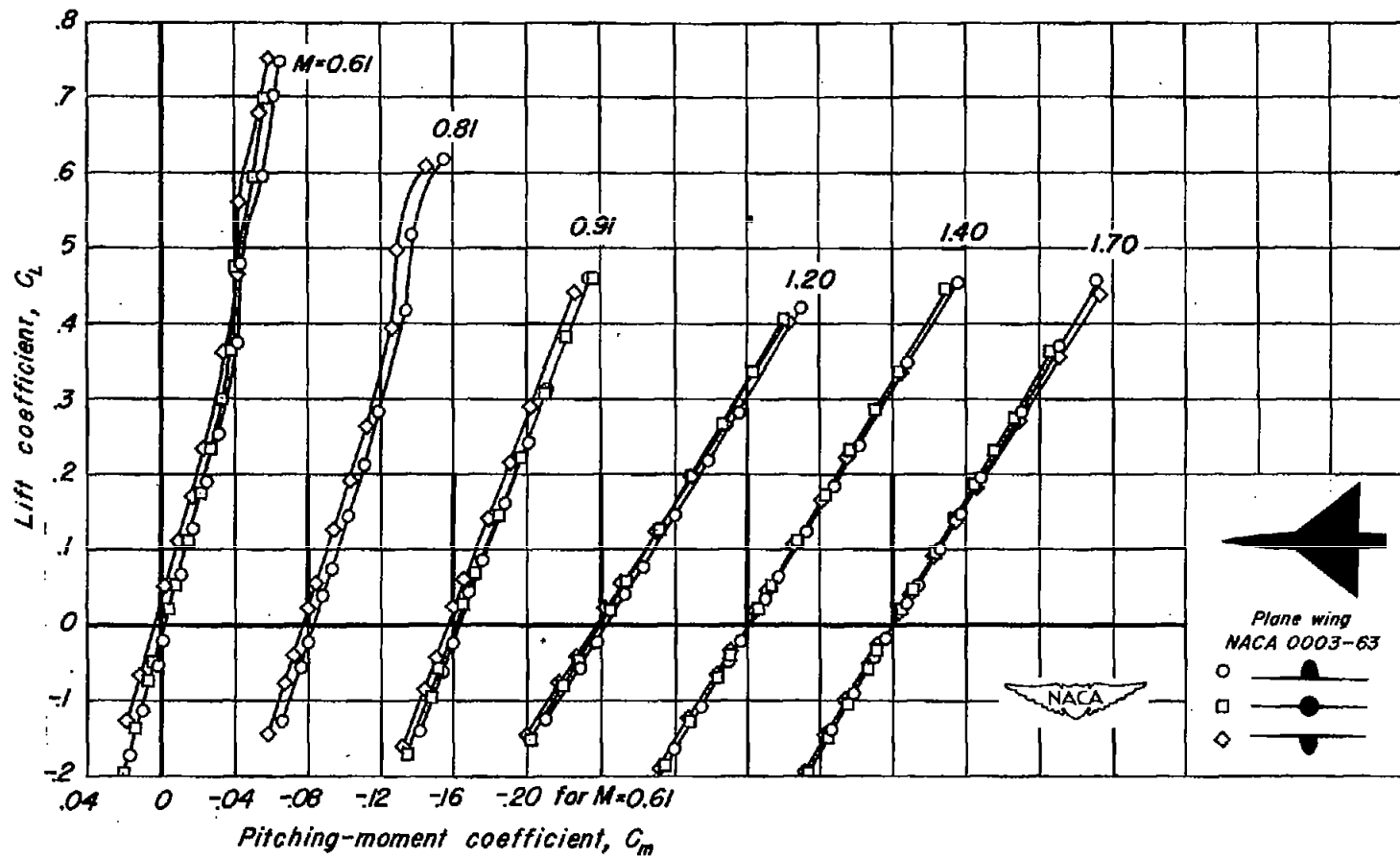
(a) C_L vs α

Figure 10.-The variation of the aerodynamic characteristics with lift coefficient for three vertical positions of the triangular wing at various Mach numbers, Reynolds number 4.8 million.



(b) C_L vs C_m

Figure 10.-Continued.

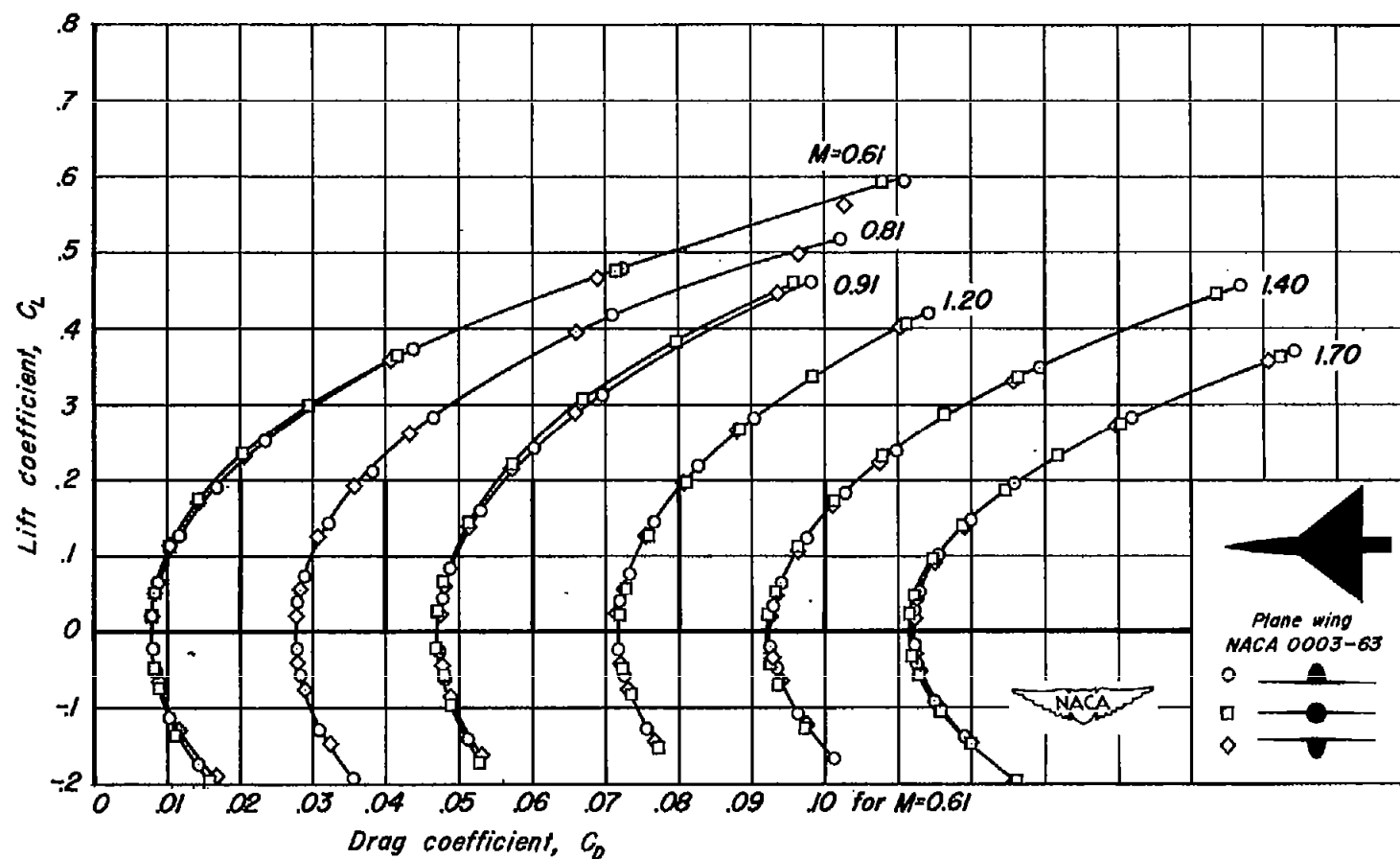
(c) C_L vs C_D

Figure 10.-Continued.

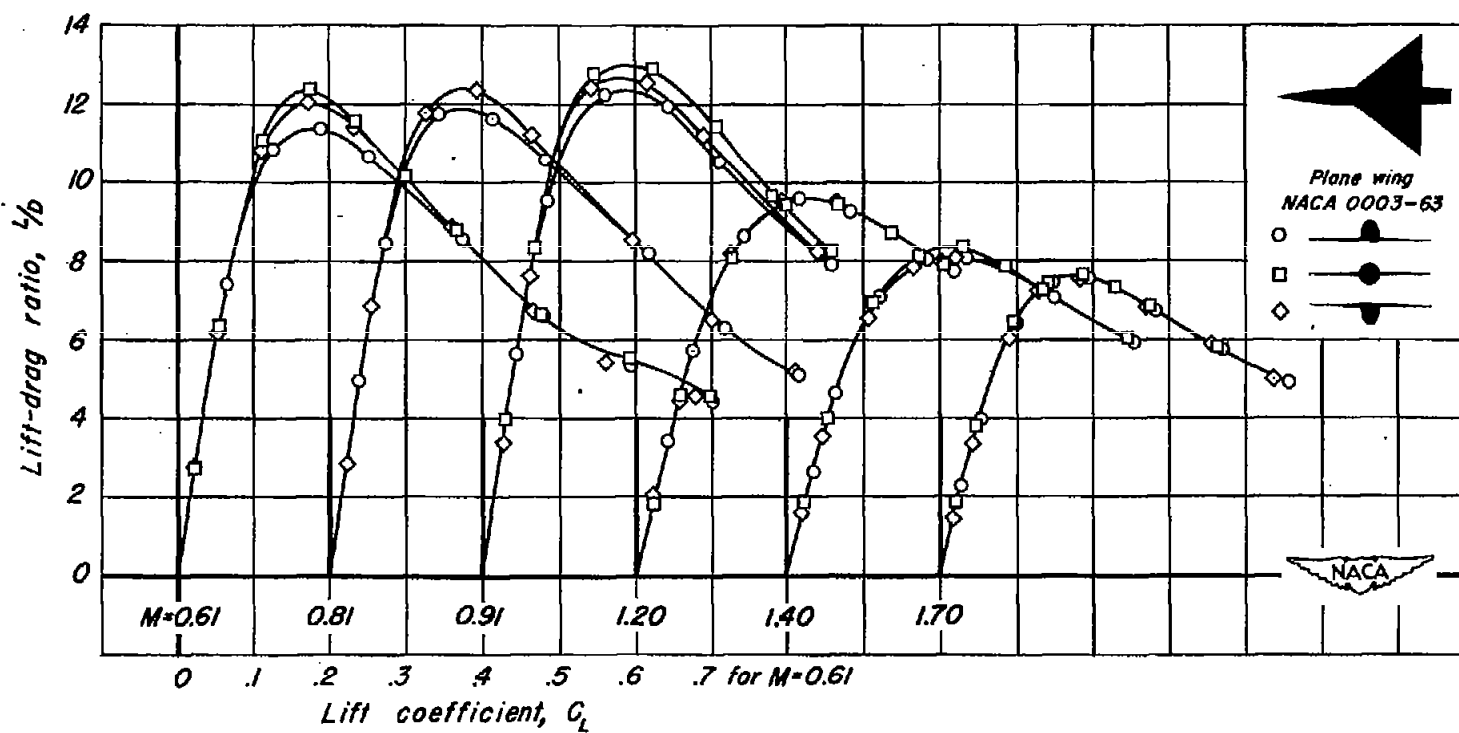


Figure 10.- Concluded.

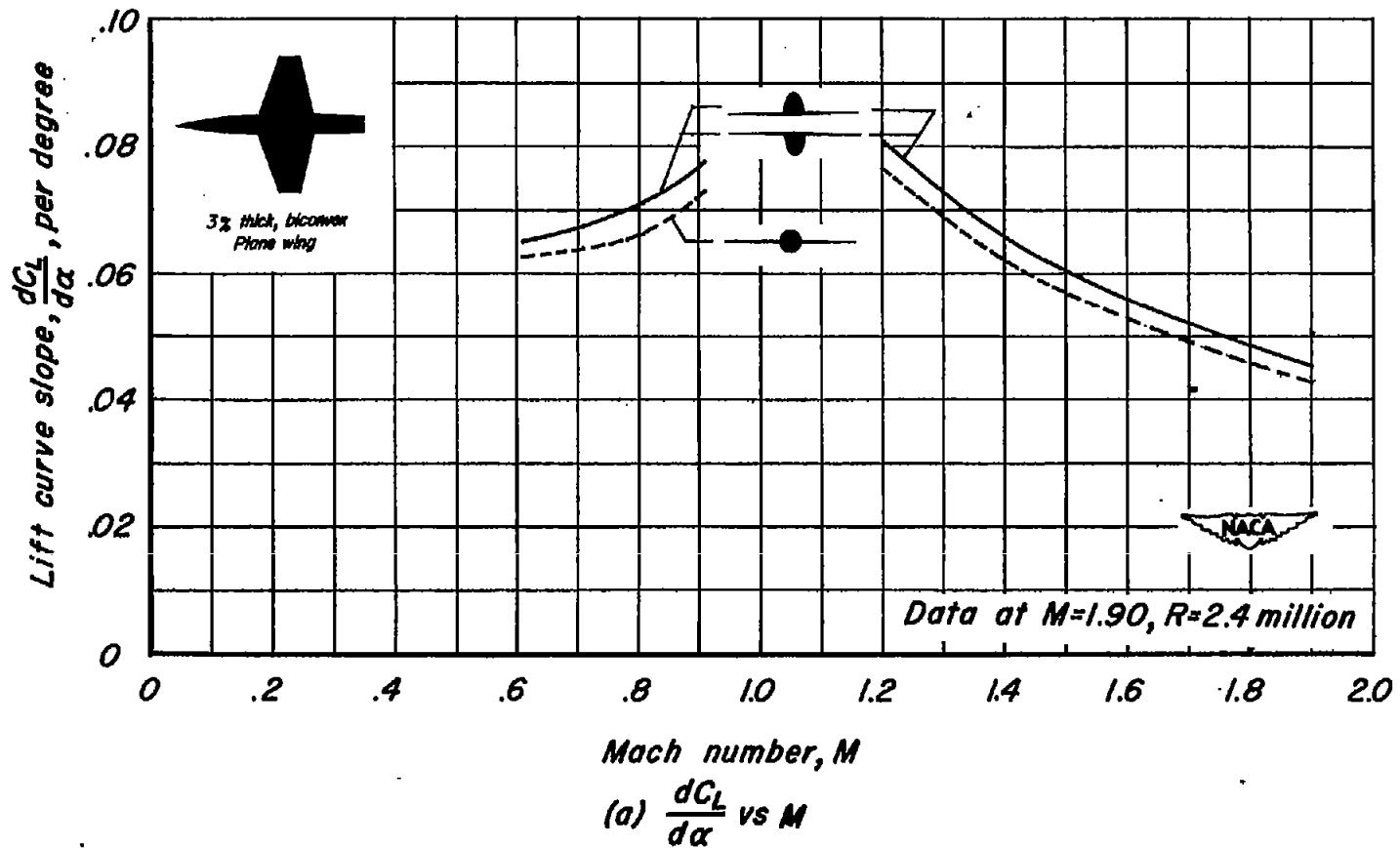


Figure 11.—Summary of the aerodynamic characteristics as a function of Mach number for three vertical positions of the unswept wing. Reynolds number, 3.8 million.

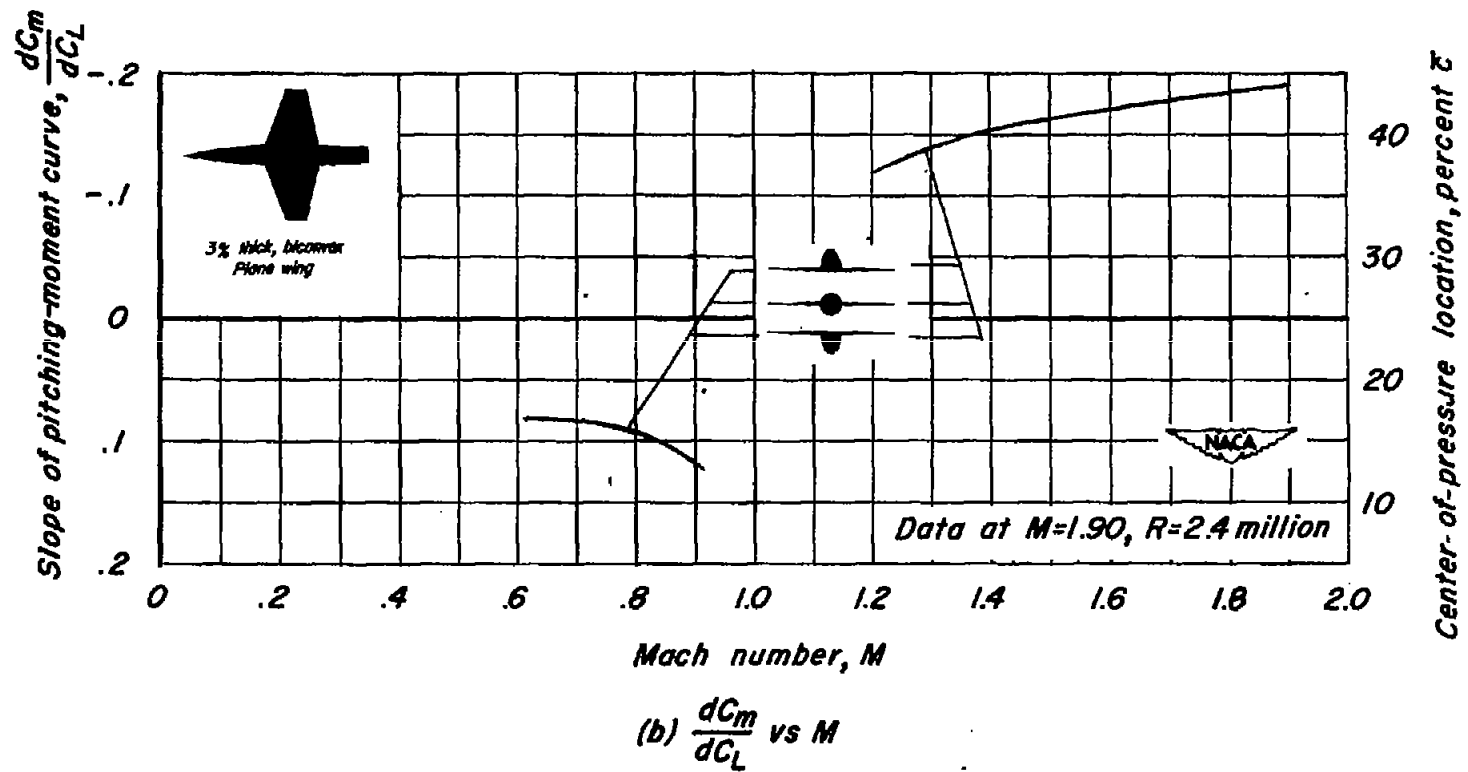


Figure 11.- Continued.

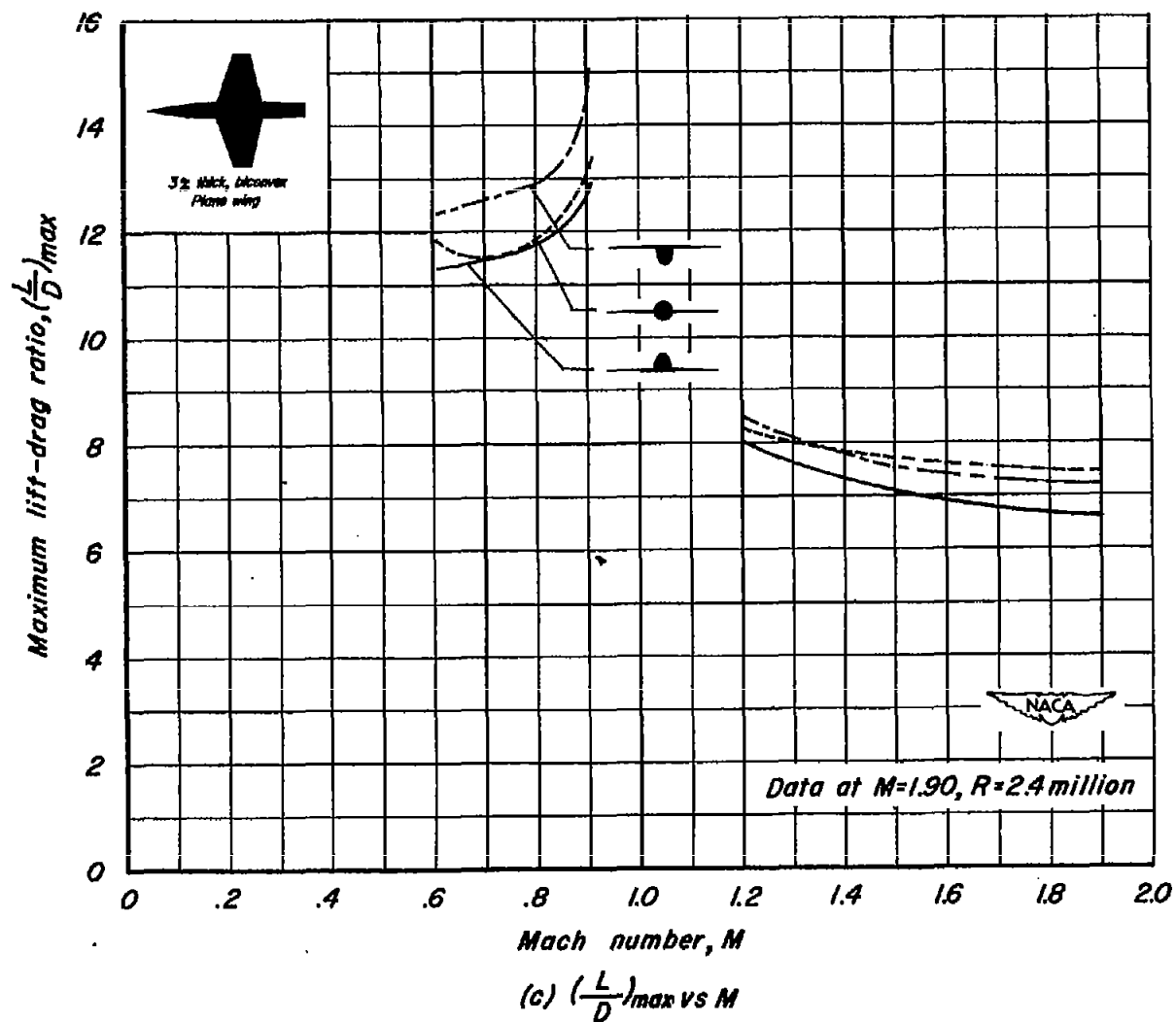


Figure 11.- Continued.

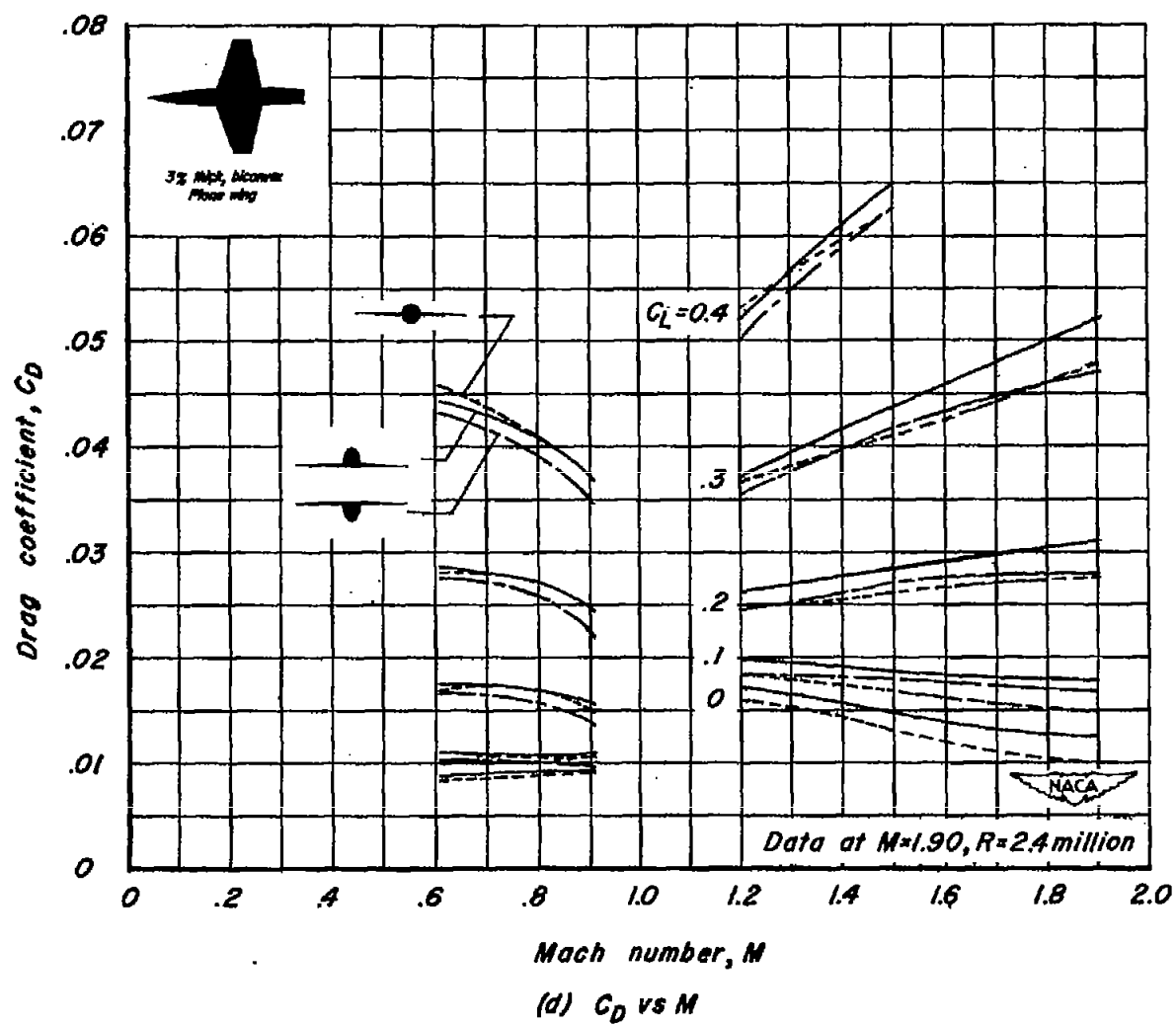


Figure 11. - Concluded.

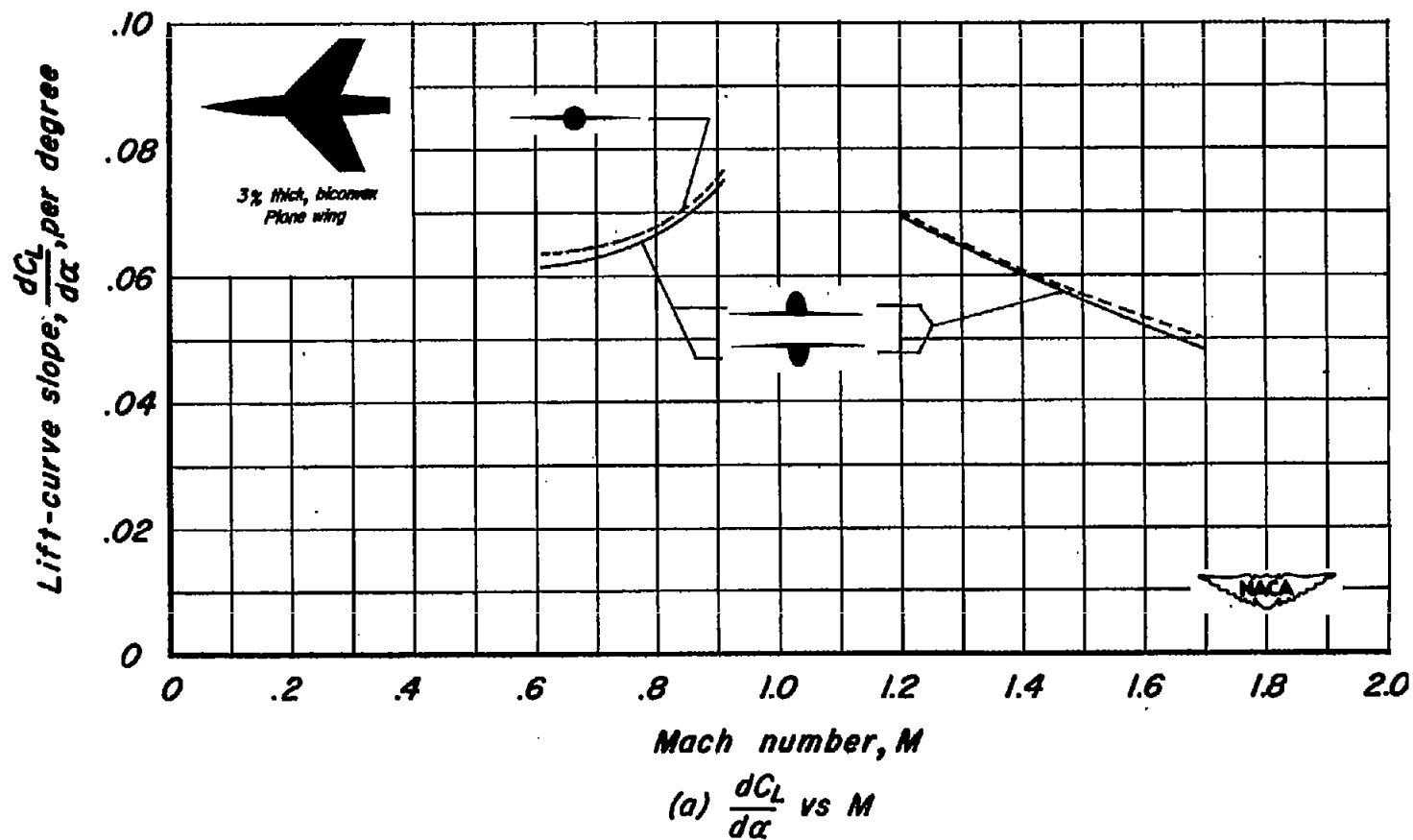


Figure 12.—Summary of the aerodynamic characteristics as a function of Mach number for three vertical positions of the swept-back wing. Reynolds number, 3.8 million.

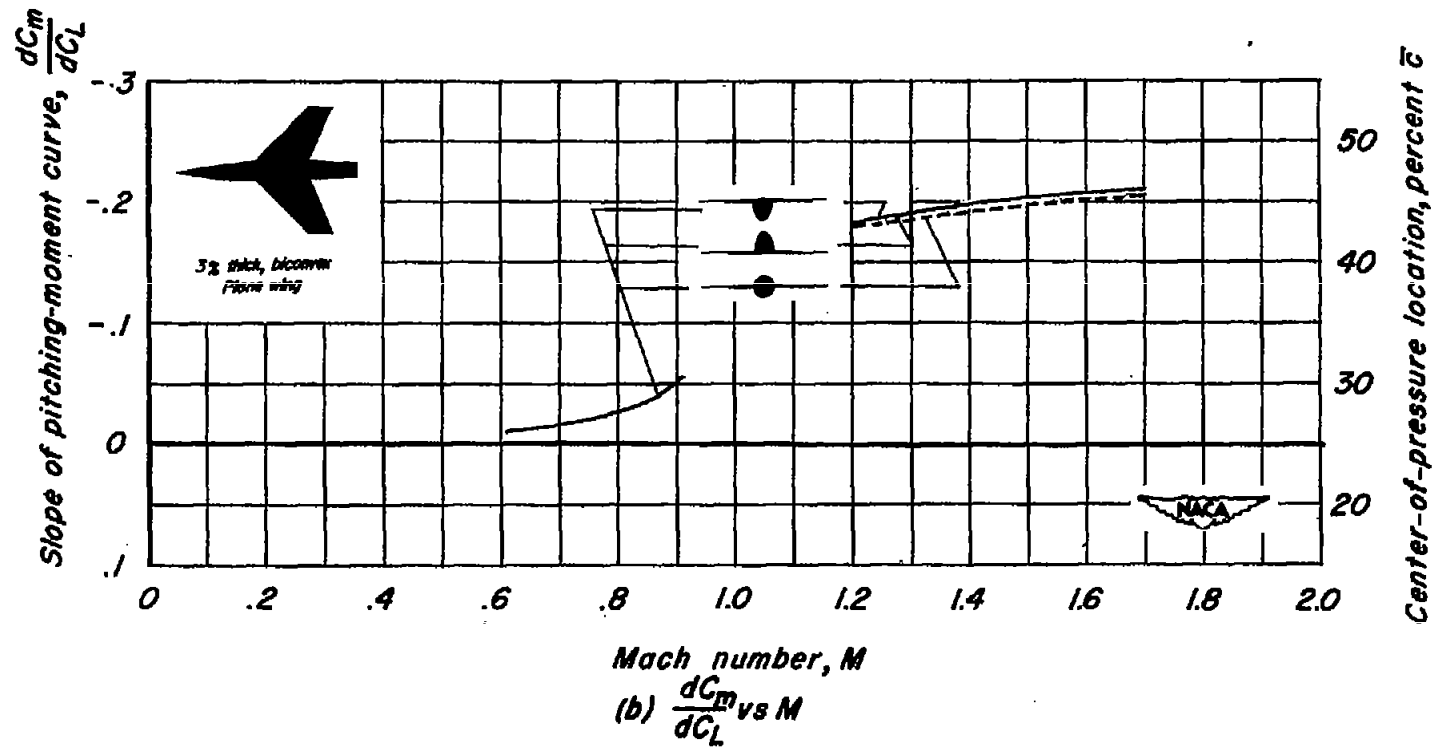


Figure 12.-Continued.

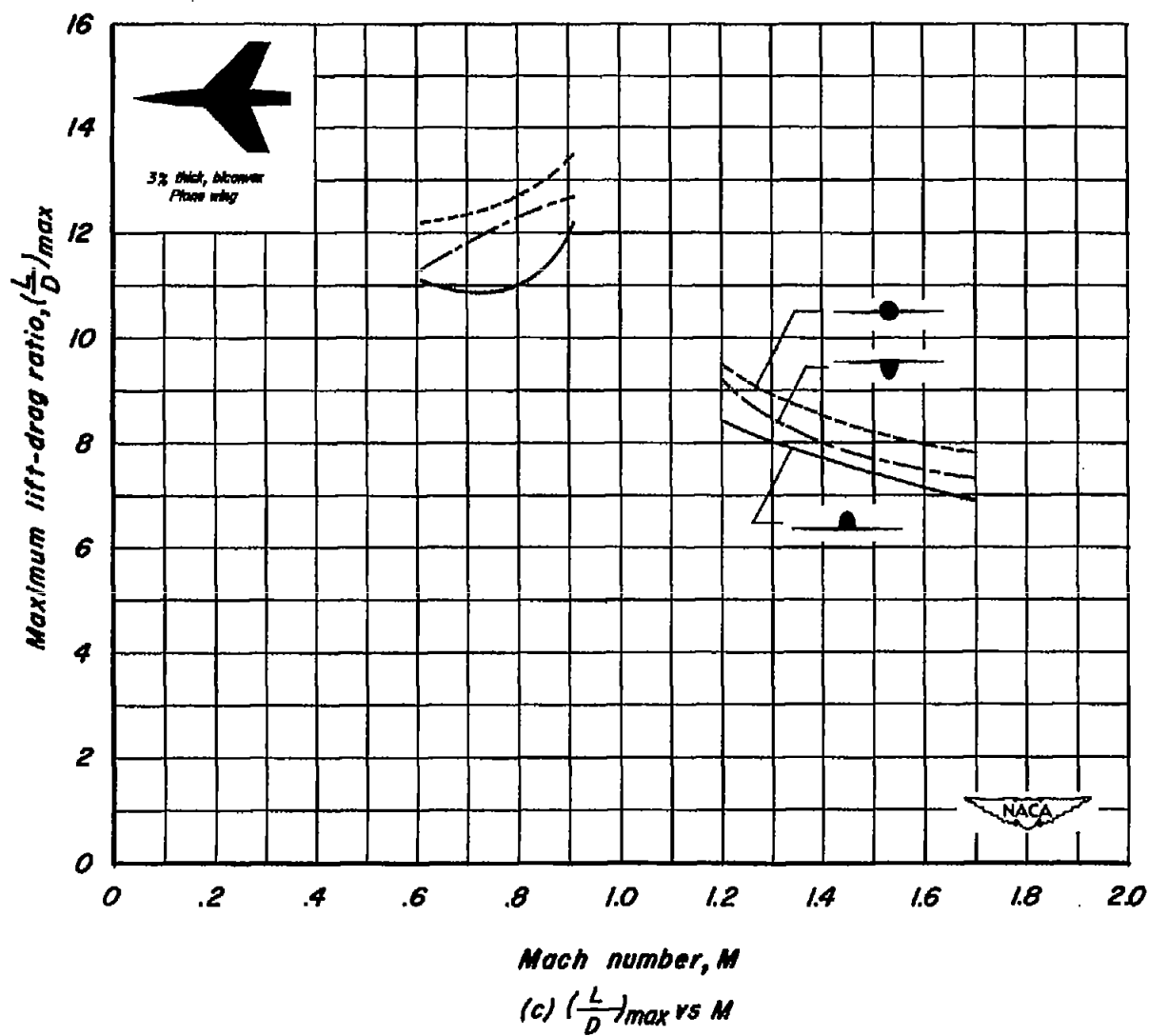


Figure 12.-Continued.

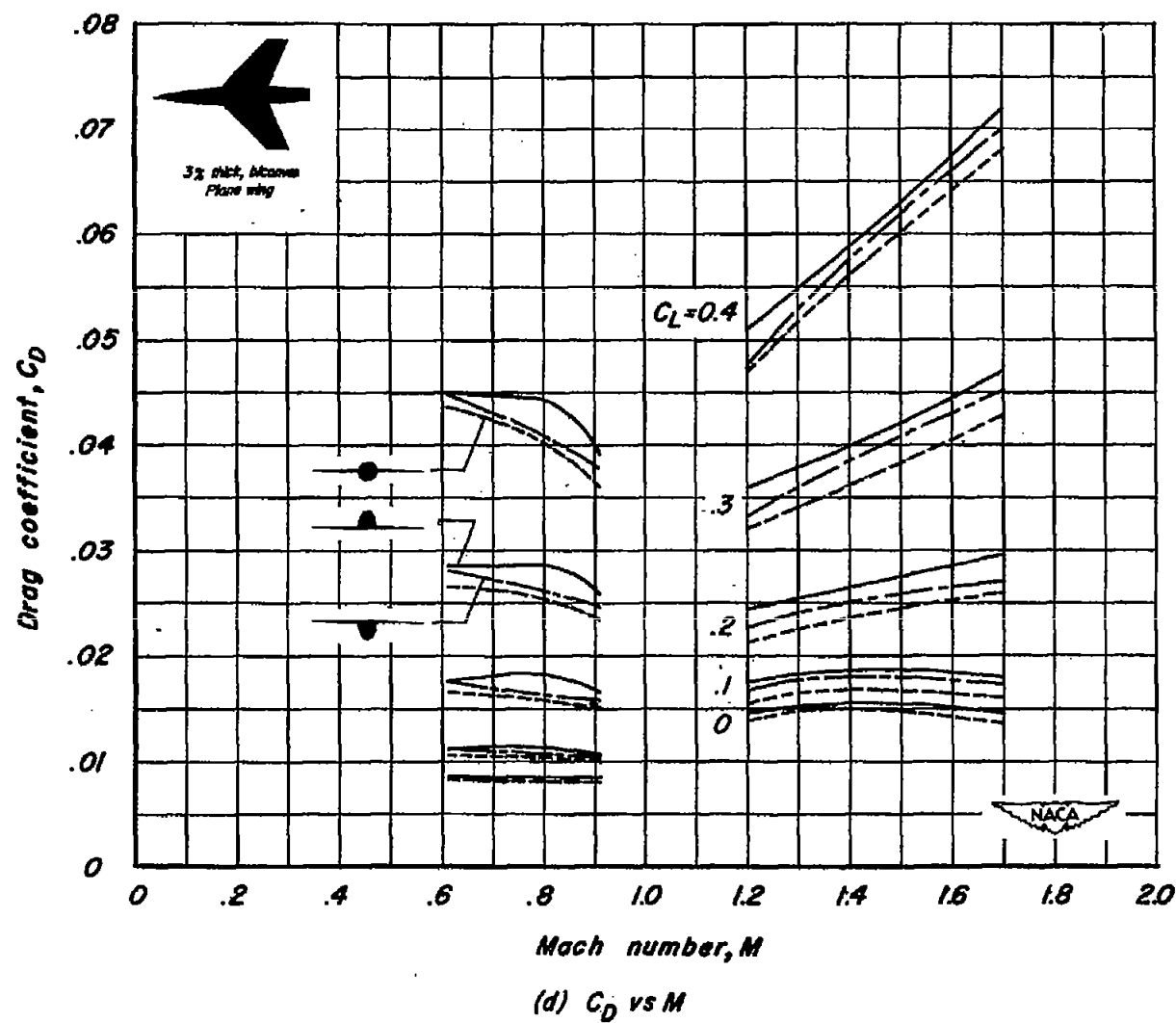


Figure 12.—Concluded

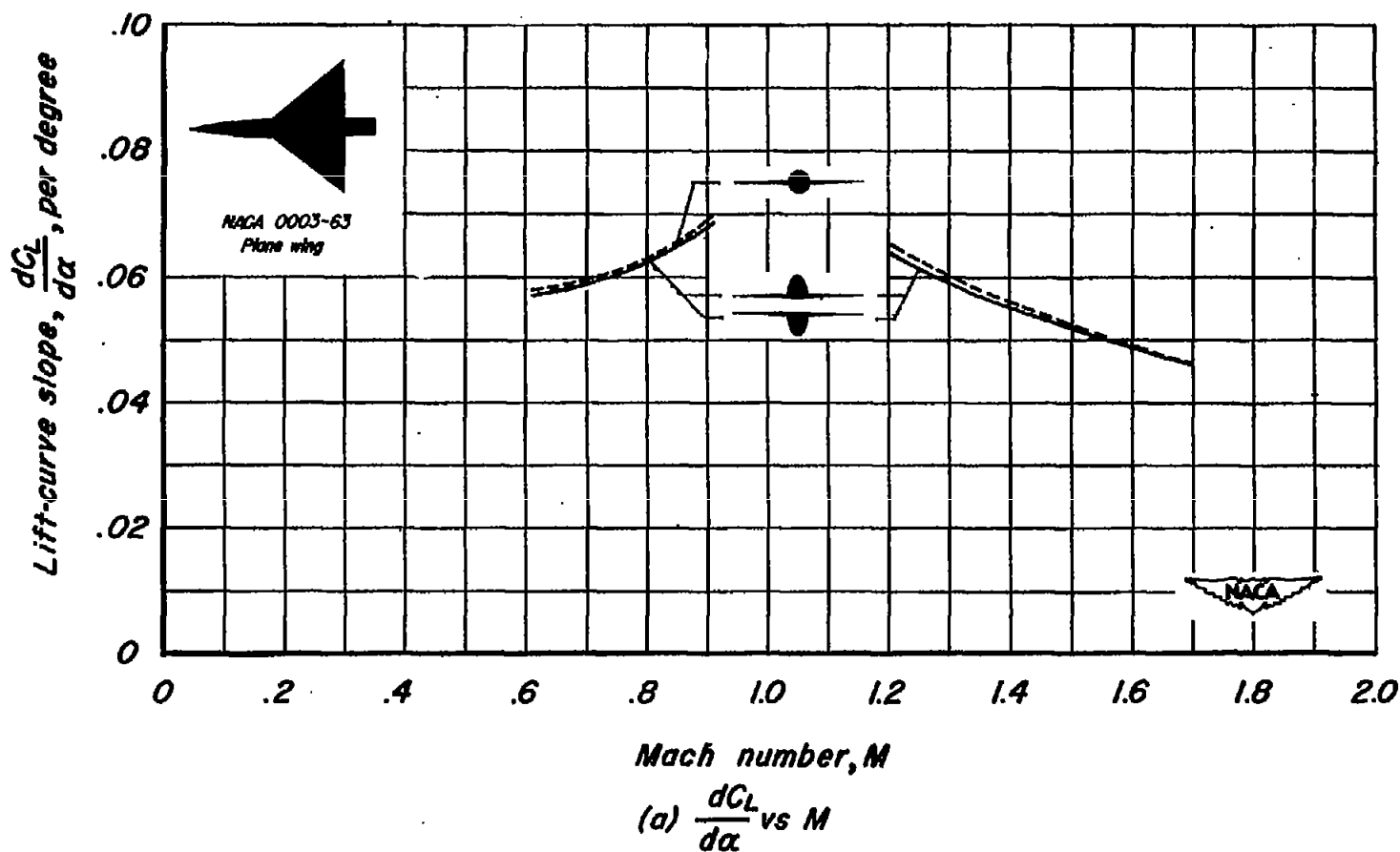


Figure 13.-Summary of the aerodynamic characteristics as a function of Mach number for three vertical positions of the triangular wing. Reynolds number, 4.8 million.

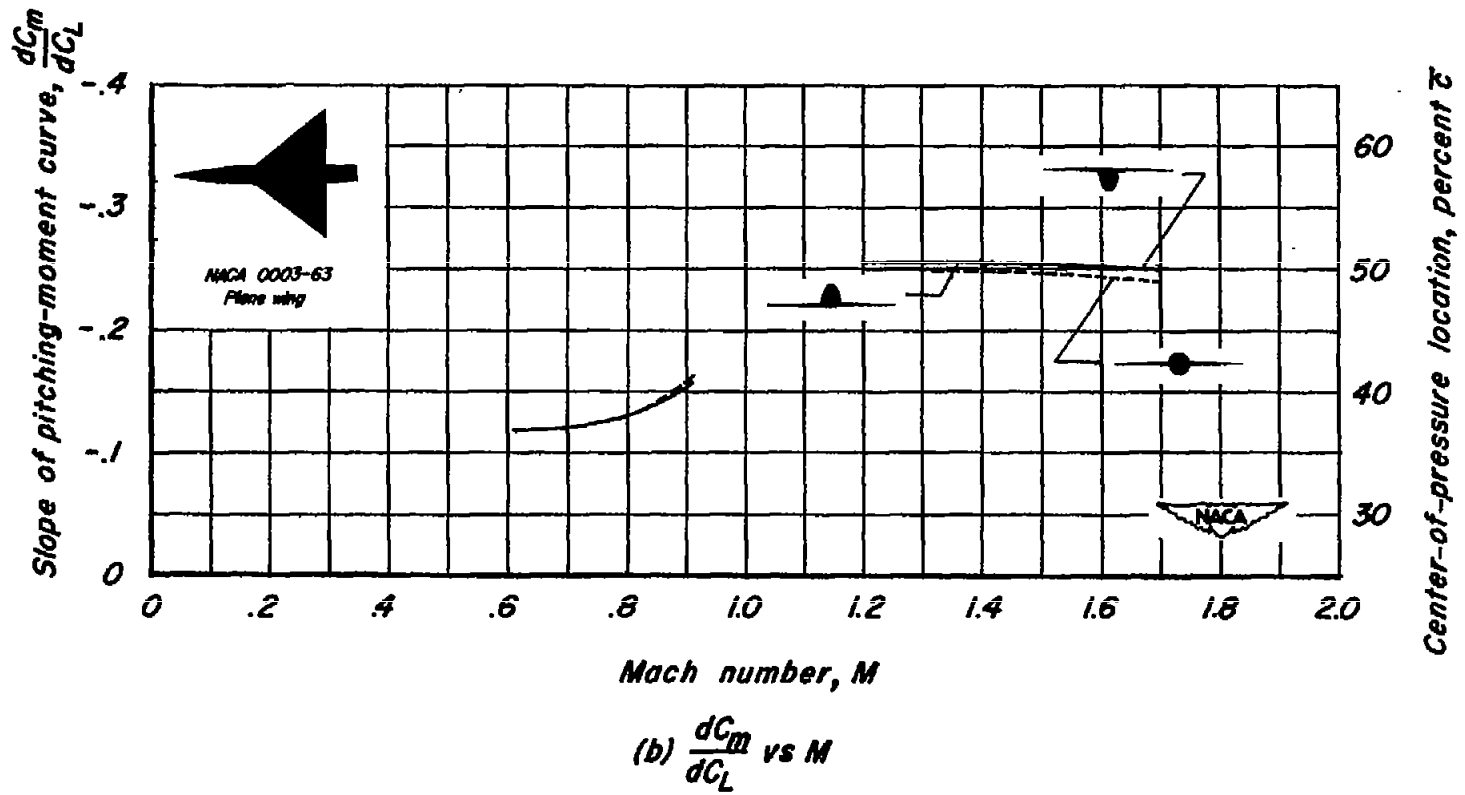
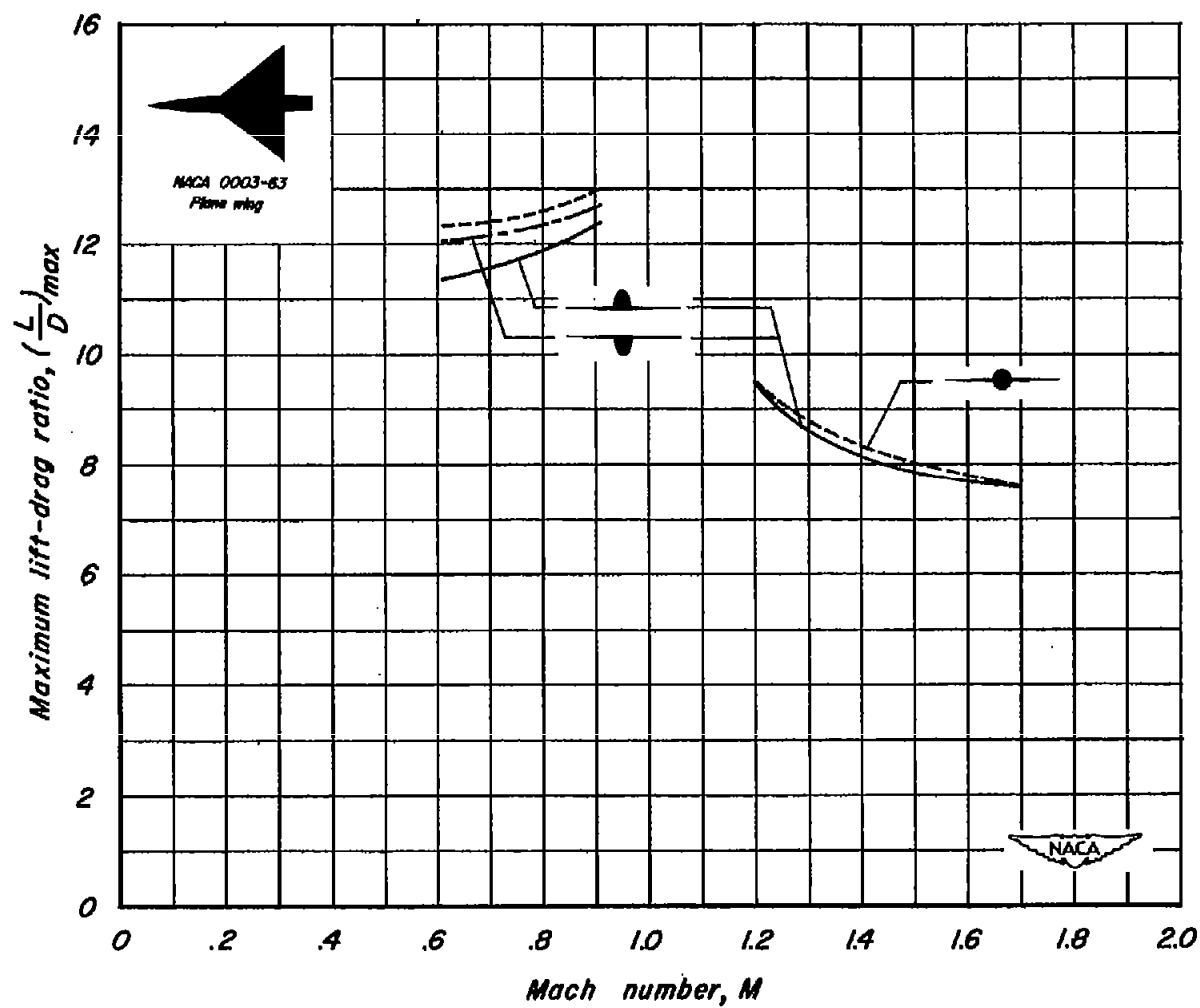
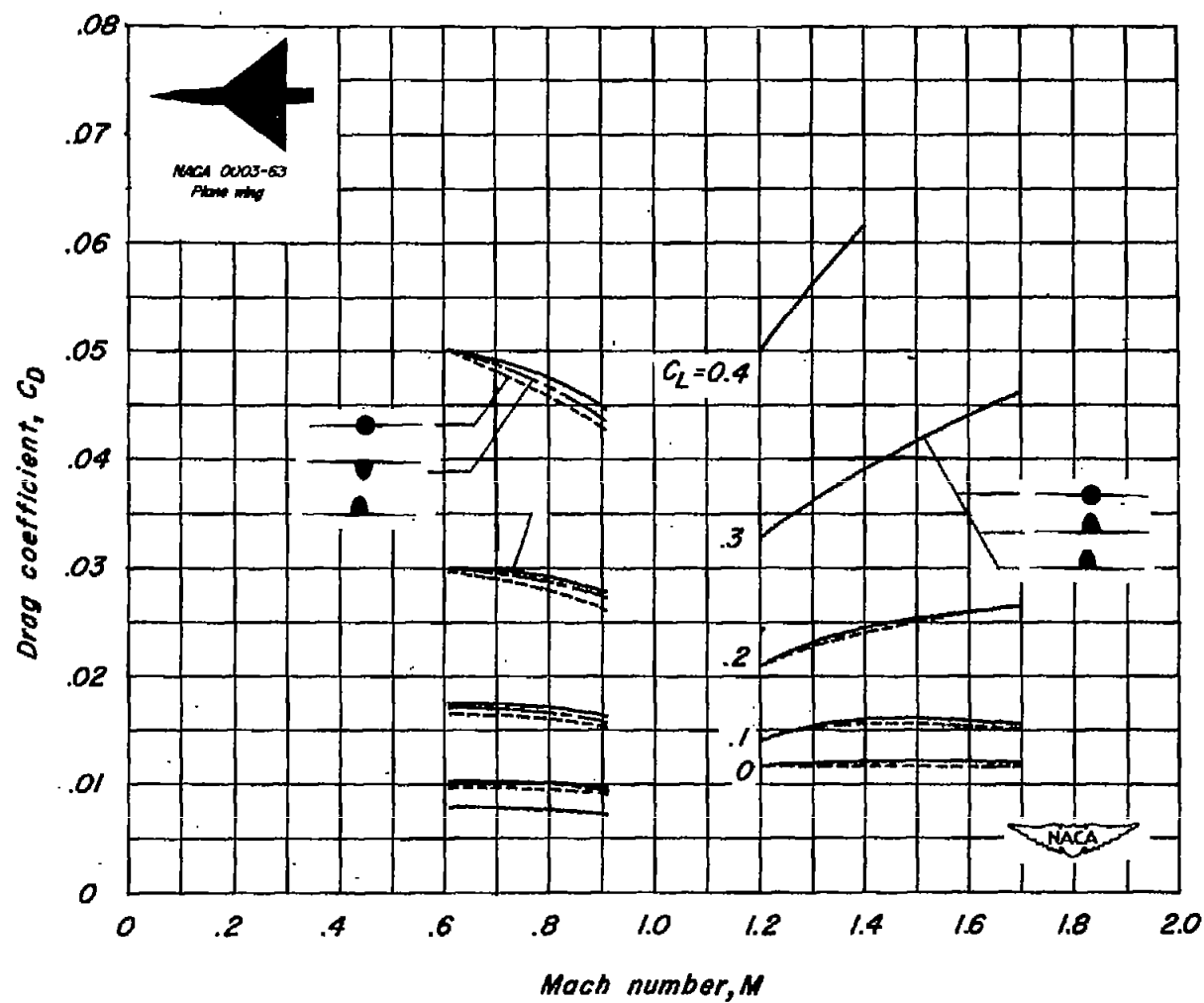


Figure 13.-Continued.



(c) $(\frac{L}{D})_{max}$ vs M

Figure 13. - Continued.



(d) C_D vs M

Figure 13.- Concluded.